CellPress

Neuron
Article

Multisensory Integration in the Mouse Striatum

Ramon Reig[1,*] and Gilad Silberberg[1,*]
[1]Department of Neuroscience, Karolinska Institute, Stockholm 17177, Sweden
*Correspondence: ramon.reig@ki.se (R.R.), gilad.silberberg@ki.se (G.S.)
http://dx.doi.org/10.1016/j.neuron.2014.07.033

SUMMARY

The basal ganglia are involved in sensorimotor functions and action selection, both of which require the integration of sensory information. In order to determine how such sensory inputs are integrated, we obtained whole-cell recordings in mouse dorsal striatum during presentation of tactile and visual stimuli. All recorded neurons responded to bilateral whisker stimulation, and a subpopulation also responded to visual stimulation. Neurons responding to both visual and tactile stimuli were located in dorsomedial striatum, whereas those responding only to whisker deflections were located dorsolaterally. Responses were mediated by overlapping excitation and inhibition, with excitation onset preceding that of inhibition by several milliseconds. Responses differed according to the type of neuron, with direct pathway MSNs having larger responses and longer latencies between ipsilateral and contralateral responses than indirect pathway MSNs. Our results suggest that striatum acts as a sensory "hub" with specialized functional roles for the different neuron types.

INTRODUCTION

Integrating sensory information and producing the appropriate motor output are the basic functions of the nervous system, and the neural networks underlying these two functions are tightly linked. The basal ganglia are involved in various functions, including motor learning, planning, and execution, as well as in decision making and reward (Haber, 2008; Middleton and Strick, 2000; Schultz et al., 1997), all of which require integration of sensory information. The input layer of the basal ganglia, striatum, receives glutamatergic inputs from multiple cortical areas, including sensory, motor, and prefrontal cortices (Alloway et al., 2009; Hoover et al., 2003; Kincaid and Wilson, 1996; Wilson, 1987). These projections are characterized by a high degree of divergence and convergence (Flaherty and Graybiel, 1991), enabling striatal neurons to integrate inputs from different cortical areas and modalities (Chudler et al., 1995; Nagy et al., 2005, 2006; Wilson et al., 1983). Corticostriatal projections originate from both hemispheres and are mediated by different subtypes of pyramidal neurons (Carman et al., 1965; Kress et al., 2013; Künzle, 1975; Lei et al., 2004; Wall et al., 2013), suggesting that striatal neurons may receive bilateral sensory input with different synaptic properties. Striatal neurons respond to sensory input from different modalities such as tactile, auditory, and visual input (Brown et al., 1996; Nagy et al., 2005; Schulz et al., 2009; Wilson et al., 1983). Due to the high convergence in the corticostriatal pathway and the loose topographical correspondence (Kincaid et al., 1998), individual striatal neurons may be involved in tactile-visual sensory integration; however, such synaptic integration at the single neuron level has not yet been shown in striatum.

Striatal projection neurons (MSNs) are divided into two main subpopulations according to their projection via the direct or indirect pathway (Alexander and Crutcher, 1990; Smith et al., 1998), with direct pathway neurons facilitating motor activity and indirect pathway neurons inhibiting it (Albin et al., 1989; Kravitz et al., 2010). Both subpopulations receive cortical as well as thalamic inputs (Doig et al., 2010); however, it has been debated whether contralateral and ipsilateral corticostriatal projections are selective or biased in targeting direct and indirect pathway MSNs, respectively (Kress et al., 2013; Lei et al., 2004; Reiner et al., 2010; Wall et al., 2013). Corticostriatal synapses formed onto direct and indirect pathway neurons and interneurons have different properties (Calabresi et al., 1996; Fino and Venance, 2011; Kreitzer and Malenka, 2008; Surmeier et al., 2007), suggesting that striatal neurons of different types may also respond differently to sensory input in vivo.

MSNs recorded in vivo are characterized by low discharge frequencies (Adler et al., 2012; Berke et al., 2004; Wilson, 1993), suggesting that a large fraction of their synaptic inputs are subthreshold and do not often contribute to action potential discharge. We therefore used whole-cell striatal recordings in order to study synaptic responses to tactile and visual stimuli. We show that neurons throughout dorsal striatum respond to bilateral whisker stimulation in a type-dependent manner and that neurons in dorsomedial striatum perform multisensory integration.

RESULTS

Whole-Cell Recordings in Dorsal Striatum

Whole-cell patch-clamp recordings were obtained from neurons in dorsolateral striatum (n = 59 neurons), dorsomedial striatum (n = 50 neurons), and layer V of S1 barrel field (n = 20 neurons). Of all recorded neurons (n = 129), 45 were stained and morphologically reconstructed (see Experimental Procedures), three of which were cortical pyramidal neurons and 42 were striatal neurons. Striatal neurons were located between 1,854 and 2,613 μm below the pia, and the average recording time for all neurons was 48 ± 20 min (minimum = 9 min, maximum = 100 min; n = 129). The striatal regions targeted for recordings were selected

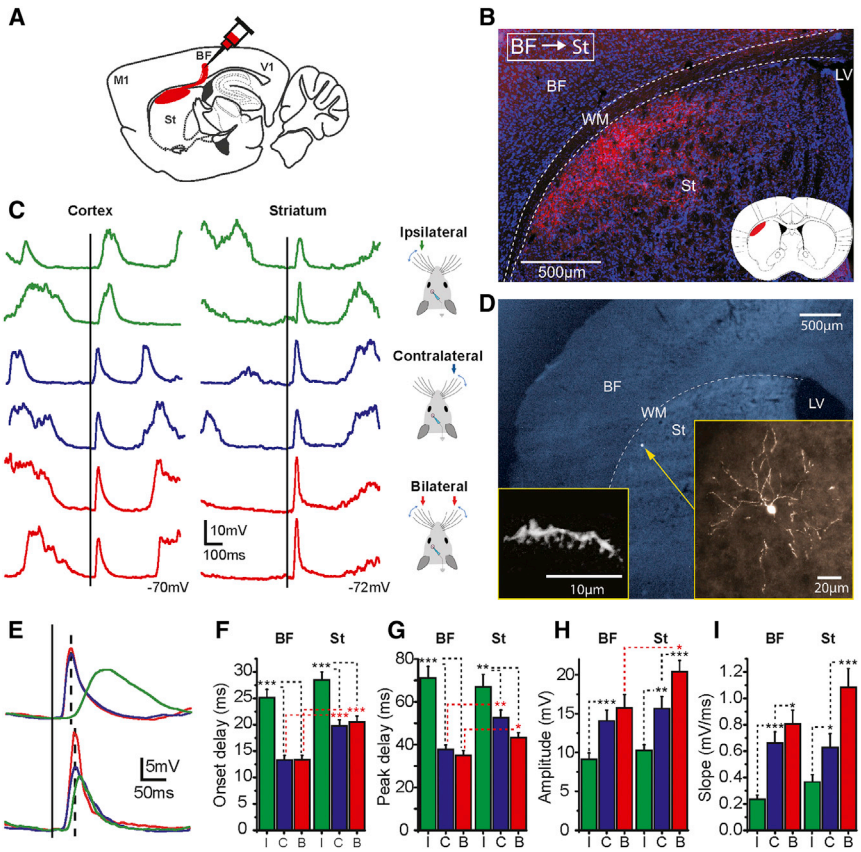

Figure 1. Striatal Integration of Bilateral Whisker Deflections

(A) Schematic of anterograde tracing (BDA) injection in layer 5 of cortical S1 (barrel field: BF).

(B) Example of ipsilateral axonal projection from cortical S1 to striatum. BDA staining: axonal projections (red), Nissl staining (blue). Inset illustrates the axonal projection field in striatum marked on the coronal diagram taken from Paxinos mouse brain atlas at the AP 0 mm coordinate (in red).

(C) Raw traces of responses to bilateral whisker deflection in cortical (left) and striatal MSN (right) during down states.

(D) Morphological reconstruction of the striatal MSN recorded in (C). The different scales show the neuron position (yellow narrow), morphology and its dendritic spines.

(E) Waveform average of the responses for the two neurons showed in (C).

(F–I) Average responses of cortical and striatal neurons to whisker deflection as recorded during down states. Ipsilateral in green, contralateral in blue, and bilateral stimulation in red. Onset delay (F), peak delay (G), amplitude (H), and slope (I). Cortical neurons n = 17; striatal MSN n = 20. Only recordings in (C)–(I) were obtained using 30 mM chloride in the intracellular solution.

Error bars represent the SEM and asterisks *, **, and *** represent p values smaller than 0.05, 0.01, and 0.001, respectively.

according to the existence of corticostriatal projections from primary somatosensory and visual cortices (S1 and V1, respectively) following anterograde tracing (see Experimental Procedures; Figures 1A, 1B, 3A, and 3B). As described in previous studies (Alloway et al., 1999, 2006; McGeorge and Faull, 1987; Pidoux et al., 2011; Wright et al., 2001), projections from S1 (barrel field) were found throughout the dorsal striatum, with higher concentration in dorsolateral striatum (Figures 1B; Figure S1 available online). Projections from visual cortex, on the other hand, were located dorsomedially in proximity to the lateral ventricle (Figure 3B), in agreement with previous reports in other species (Donoghue and Herkenham, 1986; Faull et al., 1986; Norita et al., 1991; Serizawa et al., 1994).

All recorded cortical and striatal neurons exhibited slow wave oscillations (Figures 2A, 3C, S4, S6, and S7) with bimodal distribution of the membrane potential (Figures S4 and S7), as previously described (Wilson and Kawaguchi, 1996). Striatal neurons, however, had longer up state durations than cortical neurons and rarely discharged action potentials, unlike cortical neurons, which discharged several APs during up states (Figure S4). The input resistance of recorded neurons was extracted using step current injections and was calculated separately for up and down states (Figures S4F, S4H, and S4I). Unlike cortical neurons, striatal neurons had higher input resistance at up states and at more depolarized membrane potentials (Figure S4F), suggesting that inward rectification in MSNs (Kita et al., 1984; Nisenbaum and Wilson, 1995) is the dominant factor determining their input resistance as recorded at the soma, even in the presence of the synaptic barrages occurring during the UP states.

Bilateral Sensory Integration in Dorsolateral Striatum

In order to study bilateral sensory integration, we delivered brief air puffs to the whisker pads on both sides (see Experimental Procedures) and recorded subthreshold responses to ipsilateral, contralateral, and bilateral stimulation in dorsolateral striatal neurons. Using the same stimulation protocol, we compared the whisker-evoked responses in striatal MSNs to cortical regular spiking neurons (putative pyramidal cells) in layer 5 of the barrel cortex (Figures 1 and S2; Table 1). All recorded neurons responded to both ipsilateral and contralateral whisker stimulation (cortical n = 17; striatal MSNs n = 20). Sensory responses were classified according to those occurring during "Up" or "Down" states, including cases in which sensory stimulation triggered state transitions (Reig and Sanchez-Vives, 2007) (Figure 1 and S2, respectively). Response onset delays were significantly longer for ipsilateral than contralateral whisker stimulation in both cortical and striatal neurons (BF ipsilateral: 25.11 ± 6.49 ms, contralateral: 13.32 ± 3.61 ms, $p < 0.001$, n = 17; dorsolateral striatum ipsilateral: 28.45 ± 6.94 ms, contralateral: 19.78 ± 3.42 ms, $p < 0.001$, n = 20) (Figure 1F). Corresponding differences were observed also for response peak latencies (BF ipsilateral: 71.13 ± 21.98 ms, contralateral: 37.75 ± 8.52 ms, $p < 0.001$, n = 17; striatum ipsilateral: 66.88 ± 26.07 ms, contralateral: 52.62 ± 15.82 ms, $p < 0.01$, n = 20)

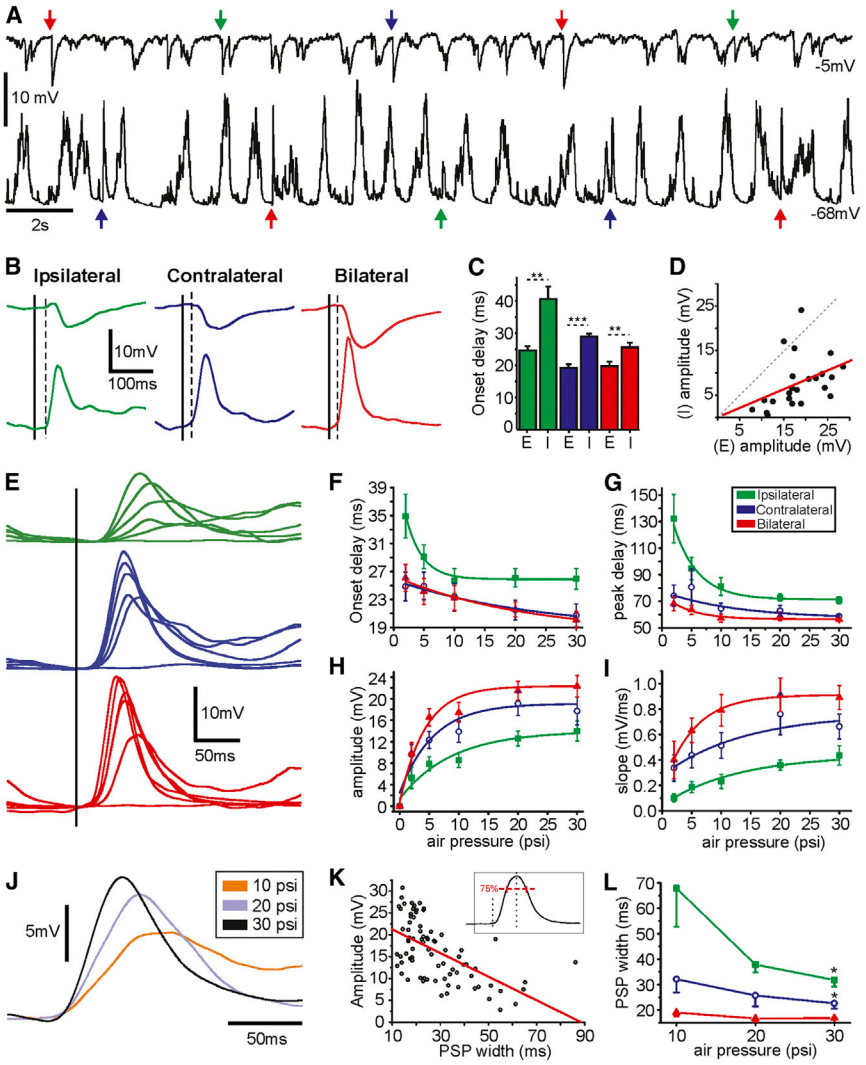

Figure 2. Excitatory and Inhibitory Components of Whisker-Evoked Responses

(A) An example of raw traces from MSN recorded at depolarized (up) and hyperpolarized membrane potential (bottom). Colored arrows show the trigger time for each type of air puff stimulation (same color code).

(B) Waveform average of the evoked responses showed in (A). Solid lines represent the stimulation onset, and dashed lines illustrate the onset of the excitatory response components.

(C) Average onset delay of the excitatory (E) and inhibitory (I) response components; n = 8.

(D) Amplitudes of excitatory and inhibitory components of responses to ipsilateral, contralateral, and bilateral whisker stimulation ($p = 0.04$, $R = 0.41$, n = 8 neurons).

(E) Waveform average of MSN responding to different stimulus intensities (air pressure intensities: 0, 2, 5, 10, 20, and 30 psi).

(F–I) Averages of striatal MSNs in respond to the same stimulus intensities showed in (E). Onset delay (F), peak delay (G), amplitude (H), and slopes (I); n = 9. All responses to whisker deflection are measured during down states. Color code for graphs and traces; ipsilateral (green), contralateral (blue), and bilateral (red) whisker stimulation. Asterisks *, **, and *** represent p values smaller than 0.05, 0.01, and 0.001, respectively.

(J) Waveform average of MSN responding to ipsilateral whisker stimulation at different stimulus intensities (air pressure intensities: 10, 20, and 30 psi).

(K) Amplitudes versus PSPs width of responses measured at 75% of the maximal amplitude, as inset shows (linear relation $p < 0.001$, $R = -0.58$, n = 81 from nine neurons responding to ipsilateral, contralateral, and bilateral stimulation at 10, 20, and 30 psi).

(L) Averages comparing the PSP width for contralateral (blue), ipsilateral (green), and bilateral stimulation (red) in response to 10, 20, and 30 psi puff stimulation. Significant differences between 10 and 30 psi for ipsilateral and contralateral stimulation ($p < 0.05$, n = 9); note that stronger puff stimulation induces shorter responses in striatal MSNs. Error bars represent the SEM and asterisks *, **, and *** represent p values smaller than 0.05,0.01, and 0.001, respectively.

(Figure 1G). Onset and peak latencies in response to contralateral and bilateral stimulation were significantly shorter in cortical neurons (Figures 1F and 1G). Response amplitudes for both cortical and striatal neurons were always larger when occurring during down states than during up states (Figures 1H and S2F, respectively). Contralateral whisker stimulation evoked larger amplitudes than ipsilateral stimulation in both cortical and striatal neurons (cortex during down states, ipsilateral: 9.11 ± 3.41 mV, contralateral: 14.07 ± 5.67 mV, $p < 0.001$; striatum during down states, ipsilateral: 10.27 ± 3.27 mV, contralateral: 15.65 ± 6.90 mV, $p < 0.01$) (Figure 1H). However, when stimuli were delivered simultaneously to both sides, a significant increase in amplitude was observed in striatal responses but not in cortical ones (cortex bilateral: 15.72 ± 7.09 mV; striatum bilateral: 20.37 ± 6.52 mV, $p < 0.05$) (Figure 1H). The increase in amplitude in the striatal MSNs is also reflected in the slopes of responses to bilateral stimulation (Figure 1I), both suggesting a higher sensitivity to bilateral input in striatal MSNs than that observed in S1 layer 5 pyramidal cells. This difference could be explained by the higher temporal separation between ipsilateral and contralateral responses in cortical neurons compared to MSNs (response peak latency: cortex = 33.38 ± 21.46 ms; striatum = 14.26 ± 24.96 ms, $p < 0.05$, data not shown).

Sensory and electrically evoked excitation of striatal neurons is accompanied by inhibition (Pidoux et al., 2011), originating from striatal interneurons and MSN collaterals (Koós and Tepper, 1999; Tunstall et al., 2002). In order to decompose the excitatory and inhibitory response components, we used a low-chloride intracellular solution (see Experimental Procedures) enabling us to hold recorded neurons at the reversal potential for excitation (~−5 mV) or GABAa inhibition (~−70 mV, Figures 2A–2D). In all recorded MSNs, excitation preceded inhibition for ipsilateral, contralateral, and bilateral whisker stimulation (onset delays: ipsilateral excitation 24.63 ± 3.76 ms, inhibition 40.6 ± 9.7ms, $p < 0.01$; contralateral excitation 19.16 ± 2.8 ms, inhibition 28.98 ± 1.93 ms, $p < 0.001$; bilateral excitation

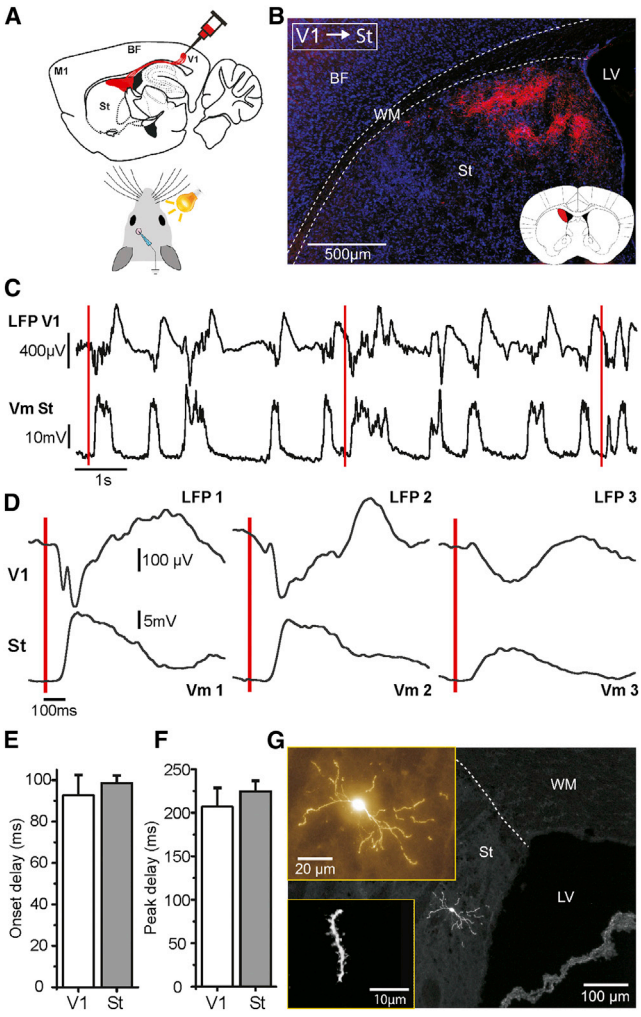

Figure 3. Striatal Integration of Visual Inputs

(A) Schematics of anterograde tracing (BDA) injection in layer 5 of primary visual cortex and experimental procedure.

(B) Example of ipsilateral axonal projection from visual cortex to striatum. BDA staining: axonal projections (red) and Nissl staining (blue). The inset illustrates the axonal projection fields in striatum (in red) marked on the coronal diagram taken from the Paxinos mouse brain atlas at the AP 0 mm coordinate.

(C) Raw traces of LFP in V1 (top) and simultaneous whole-cell recording in dorsomedial striatum (bottom). Red lines designate the onset of visual stimuli.

(D) Examples of waveform averages of three different simultaneous extra and intracellular recordings as in (C).

(E and F) Average onset and peak delays of evoked visual responses recorded simultaneously in V1 (LFP) and striatum (whole-cell), n = 16.

(G) Morphological reconstruction of a visually responding MSN in dorsomedial striatum. Different scales show the somatic location, morphology, and dendritic spines. Note the somatic location close to the lateral ventricle and white matter, within the field of ipsilateral projections from V1 (B).

Error bars represent the SEM.

19.71 ± 3.27 ms, inhibition 25.61 ± 3 ms, $p < 0.01$, n = 8) (Figure 2C). Response amplitudes were correlated, with excitatory responses followed by proportional inhibition. Regardless of the stimulus condition (ipsilateral, contralateral, or bilateral whisker stimulation), larger excitatory responses were matched by larger inhibitory ones (Figure 2D). Spontaneous activity was also mediated by mixed excitatory and inhibitory synaptic barrages during UP states, as recorded at the respective reversal potentials (Figures 2A and S4).

We next wanted to assess the stimulus intensity dependence of the different response conditions. To that end, we altered the pressure generating the air puff, resulting in different deflection intensities. The air puff duration remained constant (15 ms), and the air pressure was changed in a range between 0 and 30 psi (0, 2, 5, 10, 20, and 30 psi) (Figure 2E). For all three stimulus conditions, onset and peak delays were shortened, and amplitudes and slopes increased when air puff pressure was increased from 2 to 20 psi (Figures 2E–2I). Interestingly, response durations, measured as the width at 75% amplitude, were inversely related to the amplitudes and stimulus strength (Figures 2J–2L), possibly due to curtailing of responses by the increased inhibitory component (Figure 2D). The relationship between ipsilateral and contralateral responses was maintained for different stimulus intensities, with contralateral (and bilateral) stimulation evoking earlier onset and peak response latencies (Figures 2F and 2G), with larger amplitudes and rise slopes (Figures 2H and 2I).

Visual Responses in Dorsomedial Striatum

In order to study responses of striatal neurons to visual stimulus, we obtained whole-cell recordings from neurons in dorsomedial striatum (Figure 3). The recording area was selected according to the presence of axonal projections from cortical V1 (Figures 3A and 3B, n = 5), which were clustered in dorsomedial portions of the striatum, near the lateral ventricle (Figure 3B). Visual stimuli were presented to the contralateral eye as brief light flashes from a white LED (see Experimental Procedures) during whole-cell recordings in striatum and LFP recordings from V1. As described above, responses were sorted offline to those occurring during up or down states. The onset delay for contralateral visual responses during down states was 98.43 ± 19.05 ms (ranging between 56.7 and 141.0 ms, n = 25), almost five times longer than the onset response to whisker stimulation (19.78 ± 3.42 ms, Figure 1F) and similar to previously reported visual responses (Schulz et al., 2009, 2011). Such delays are expected when comparing to the long and variable delays (50–130 ms) described for visual responses in mouse visual cortex (Niell and Stryker, 2008; Takagaki et al., 2008). In order to verify the occurrence of cortical visual responses, we obtained extracellular recordings (LFP) in V1 simultaneously with the striatal whole-cell recordings (n = 16, Figures 3C and 3D). Onset and peak latencies were slightly earlier, although not significantly different between cortical and striatal visual responses (Figures 3E and 3F), which may be due to the large response variability. The amplitude of visual responses was 13.28 ± 5.38 mV and slopes 0.14 ± 0.15 mV/ms (data not shown, n = 25).

Multisensory Integration by Individual Striatal Neurons

Visual stimulation was tested for 38 neurons in dorsomedial and 28 in dorsolateral striatum. Visual responses were evoked in 25 of dorsomedial neurons (66%) and in none of the dorsolateral ones; however, all neurons in both regions responded to bilateral whisker stimulation (Figure 4). Figure 4C depicts the position of anatomically reconstructed neurons, in which both tactile and

Table 1. Responses to Bilateral Whisker Stimulation Recorded in Striatal MSNs and Pyramidal Neurons in Layer 5 of the Barrel Cortex

	Ipsilateral		Contralateral		Bilateral	
	Up	Down	Up	Down	Up	Down
Onset (ms)						
Cortex	24.84 ± 5.77	25.11 ± 6.49	13.2 ± 3.6	13.32 ± 3.61	15.85 ± 7.55	13.38 ± 3.42
Striatum	28.84 ± 8.14	28.45 ± 6.94	19.62 ± 4.59	19.78 ± 5.09	18.76 ± 4.75	19.78 ± 3.42
Peak (ms)						
Cortex	59.1 ± 18.62	71.13 ± 21.98	33.46 ± 8.3	37.75 ± 8.52	32.84 ± 9.85	35.07 ± 8.52
Striatum	57.6 ± 22.65	66.88 ± 26.08	46.38 ± 13.55	52.62 ± 15.82	44.13 ± 12.15	43.17 ± 10.94
Amplitude (mV)						
Cortex	1.8 ± 2.17	9.11 ± 3.4	7.27 ± 3.9	14.07 ± 5.67	6.68 ± 4.02	15.72 ± 7.09
Striatum	5.3 ± 2.92	10.27 ± 3.27	8.83 ± 4.78	15.65 ± 6.9	10.03 ± 5.64	20.37 ± 6.52
Normalized amplitude						
Cortex	0.15 ± 0.18	0.7 ± 0.25	0.53 ± 0.19	1 ± 0	0.48 ± 0.22	1.12 ± 0.46
Striatum	0.38 ± 0.23	0.82 ± 0.49	0.58 ± 0.21	1 ± 0	0.69 ± 0.39	1.45 ± 0.5
Slope (mV/ms)						
Cortex	0.12 ± 0.06	0.23 ± 0.12	0.39 ± 0.25	0.66 ± 0.35	0.42 ± 0.28	0.8 ± 0.43
striatum	0.21 ± 0.13	0.36 ± 0.24	0.4 ± 0.31	0.62 ± 0.46	0.46 ± 0.36	1.08 ± 0.63

Mean values ± SD. The normalization was done with respect to the contralateral average amplitude during down states for each neuron.

visual stimulation were presented (n = 30). All neurons that responded to visual stimuli were located medially (Figure 4C, orange points), close to the area receiving axonal projections from V1 (Figure 3B). The differences in onset and peak delays between whisker and visual sensory responses suggested that the strongest responses in striatal neurons would not occur when stimuli are presented simultaneously, but rather when visual stimulation precedes tactile stimulation. To test this prediction, we presented the whisker stimuli at different time intervals with relation to the visual stimuli (Figure 4D). Indeed, in all cases (n = 7) maximal response amplitudes were evoked when whisker deflections followed the visual stimuli synchronized to the respective response onsets (relative interval 102.11 ± 20.98 ms, Figure 4E). Multisensory responses did not summate linearly, with maximal response amplitudes smaller and earlier than those predicted by the linear sum of unimodal responses (independent whisker 13.73 ± 3.15 mV, independent visual 13.23 ± 4.66 mV, synchronized onset 18.19 ± 4.54 mV, n = 7) (Figures 4D and 4E). This sublinear summation is expected due to the proportional inhibitory component of sensory responses (Figures 2A–2D) but may also be mediated by activation of common cortical association areas (Olcese et al., 2013). As shown above neurons in both dorsolateral and dorsomedial striatum responded to whisker stimulation; however, there were notable differences in responses recorded in both striatal regions. Dorsolateral MSNs had stronger and faster responses (Figure 4F), as reflected in response amplitudes (contralateral whisker, dorsolateral striatum: 15.6 ± 6.9 mV, dorsomedial 8.4 ± 3.67 mV; bilateral dorsolateral 20.37 ± 6.52 mV, dorsomedial 10.29 ± 4.42 mV) (Figure 4H) and slopes (ipsi-dorsolateral 0.36 ± 0.24 mV/ms, dorsomedial 0.16 ± 0.08 mV/ms; contralateral dorsolateral 0.63 ± 0.46 mV/ms, dorsomedial 0.17 ± 0.09 mV/ms; bilateral dorsolateral 1.08 ± 0.63 mV/ms, dorsomedial 0.28 ± 0.18 mV/ms, dorsolateral n = 20, dorsomedial n = 24) (Figure 4I). There were no differences in onset delays (ipsi-dorsolateral 28.45 ± 6.94 ms, dorsomedial 31.8 ± 8.35 ms, p = 0.16; contra-dorsolateral 19.78 ± 5.09 ms, dorsomedial 18.24 ± 6.68 ms, p = 0.41; bilateral dorsolateral 20.49 ± 5.19 ms, dorsomedial 18.39 ± 5.71 ms, p = 0.23, data not shown); however, there were significant differences for peak delays in all conditions, reflecting the slower response rising slopes (Figure 4G). These differences in sensory responses correlate to the differences between dorsolateral and dorsomedial striatum in the density of axonal projections from primary somatosensory cortex (Figures 1B and S1). In summary, neurons located in the dorsomedial striatum integrate tactile and visual sensory inputs, with maximal responses when the respective response onsets are aligned. Dorsolateral MSNs do not respond to visual stimulation but have larger and faster responses to whisker stimulation than dorsomedial ones.

Differential Integration of Bilateral Inputs by Direct and Indirect Pathway MSNs

The large majority of striatal neurons are MSNs, projecting via the striatonigral (direct) and striatopallidal (indirect) pathways. Since these projection pathways are believed to have different roles in basal ganglia function, it is important to understand whether and how they differ in their integration of sensory input. To that end, whole-cell recorded and electrophysiological identified MSNs were subsequently immunostained with D1 antibody (see Experimental Procedures; Figures 5A, S5, and S6) in order to classify them as direct or indirect pathway MSNs. The staining allowed us to classify MSNs into D1-expressing and putative D2-expressing MSNs, which we refer to below as D2 MSNs. Using a *Drd2* BAC transgenic mouse we verified that the D1 antibody did not stain D2-EGFP MSNs (Figure S5), suggesting that recorded MSNs that were D1 negative are indeed D2 MSNs. MSN subtype identification was obtained for 28 MSNs: 15 D1 positive and 13 D2 neurons (Figures 5A and S6). While similar in most of their electrophysiological properties, D2 MSNs had higher input resistance than D1 MSNs, as

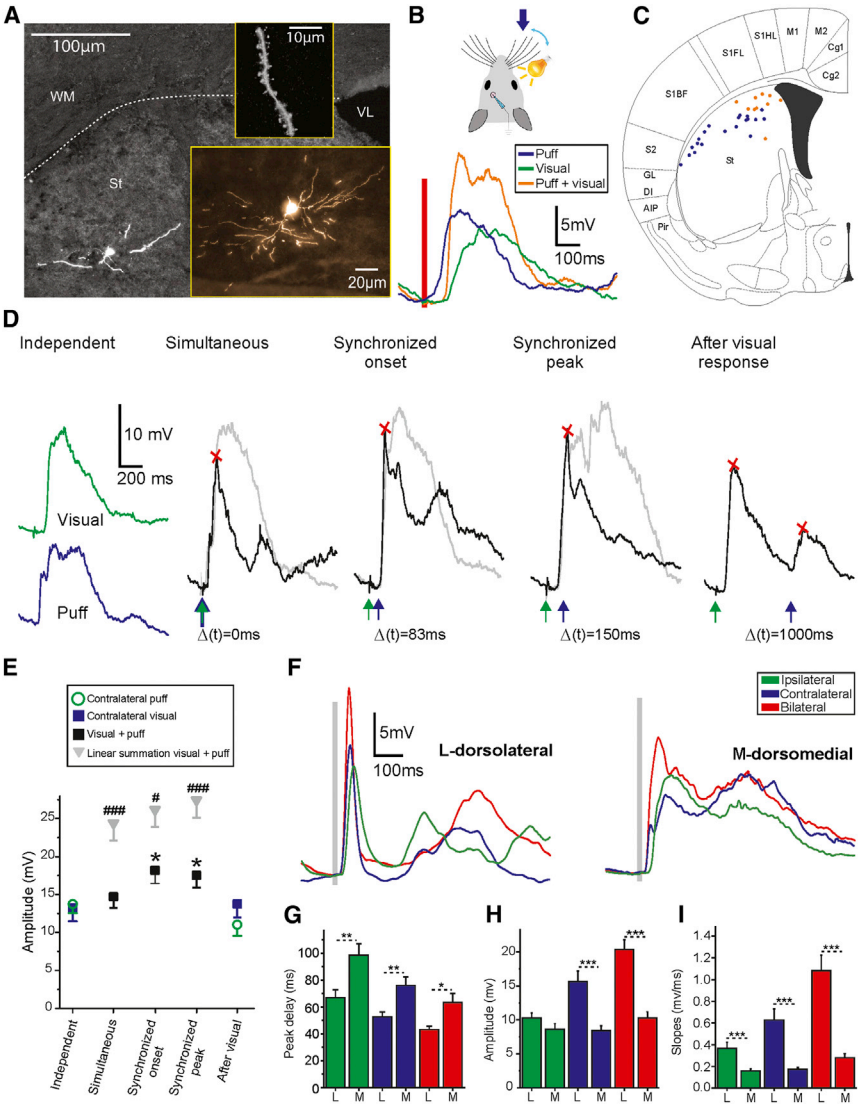

Figure 4. Striatal Integration of Visual and Tactile Inputs

(A) Morphological reconstruction of a multisensory responding MSN. Different scales show the somatic position, morphology, and dendritic spines.

(B) Schematic of the stimulation procedure (top) and waveform average of the visual, tactile, and simultaneous visual and tactile responses in the same MSN (bottom).

(C) Topographic distribution of multisensory striatal neurons. Circles represent the somatic locations of all neurons tested for both visual and whisker stimulation. All neurons (colored blue and orange) responded to whisker stimulation, and only dorsomedial neurons (marked in orange) responded to both sensory modalities. Somatic locations are overlaid on a coronal diagram taken from Paxinos mouse brain atlas at the AP 0 mm coordinate.

(D) Example of tactile and visual temporal integration. Waveform averages of evoked visual and tactile responses at different times as recorded in a dorsomedial MSN. From left to right: (1) Independent stimulation evokes visual (green) and whisker responses (blue). (2) Simultaneous visual and whisker stimulation (*dt* = 0 ms). (3) Synchronized onset of visual and whisker responses by delayed whisker stimulation (*dt* = 83 ms). (4) Synchronized peak of visual and whisker responses (*dt* = 150 ms). (5) Whisker response following visual response (*dt* = 1000 ms). The red crosses indicate the maximum amplitude of evoked response. Gray traces represent the simulated linear summation of the visual (in Green) and tactile (in blue) responses for the corresponding interstimuli intervals.

(E) Multisensory integration of visual and whisker stimuli presented at different intervals. Peak response amplitude for stimuli presented independently, simultaneously, with synchronized response onsets and peaks and with 1,000 ms relative delay (n = 7). Gray triangles represent the peak amplitude of the respective linear summation for the different intervals showing sublinear summation of the multisensory responses (#: $p < 0.05$, ###: $p < 0.001$).

(F) Waveform average of whisker responses in dorsolateral and dorsomedial MSNs.

(G–I) Average responses of dorsolateral (L) and dorsomedial (M) MSNs. n = 20 and 24, respectively. Error bars represent the SEM and asterisks *, **, and *** represent p values smaller than 0.05, 0.01, and 0.001, respectively.

measured by injection of a depolarizing and hyperpolarizing current step during down states (in MOhm, depolarized D1 112.85 ± 25.76 and D2 158.81 ± 28.93, $p < 0.001$; hyperpolarized D1 88.13 ± 27.7 and D2 107.81 ± 39.01, $p < 0.05$) (Figure 5C). Similar results were reported for D1 and D2 MSNs in recent slice studies (Gertler et al., 2008; Planert et al., 2013). Differences were also seen in their respective bilateral sensory integration. The differences in onset delays between contralateral and ipsilateral responses were significantly larger in D1 MSNs (D1 ipsi: 31.18 ± 6.49 ms, contra: 17.07 ± 7.97 ms, $p < 0.001$; D2 ipsi: 25.16 ± 3.68 ms, contra: 20.38 ± 5.35 ms, $p < 0.01$) (Figure 5D and 5E). This difference was caused by the response onset for ipsilateral stimulation that was longer in D1 than D2 MSNs (D1: 31.18 ± 6.49 ms, D2 25.16 ± 3.68 ms, $p < 0.05$) (Figures 5D and 5E; Table 2). Peak responses to contralateral and ipsilateral stimulation also had different latencies in D1 MSNs (ipsi 89.85 ± 44.44 ms, contra 63.08 ± 24.87 ms, $p < 0.01$) but were similar in D2 MSNs (ipsi 70.33 ± 23.47 ms, contra 63.71 ± 23.52 ms, $p = 0.192$) (Figures 5D, 5F and 5G). Response amplitudes were overall larger in D1 MSNs than D2 MSNs, significantly so for contralateral whisker stimulation (D1 MSNs 15.14 ± 5.47 mV, D2 MSNs 10 ± 4.93 mV, $p < 0.05$) (Figure 5H). The two MSN subpopulations also had differences in the response slopes, where D1 MSNs had faster slopes for contralateral versus ipsilateral stimuli ($p < 0.05$) but not D2 MSNs ($p = 0.13$, see Table 2; Figure 5I). Both D1 and D2 MSNs had

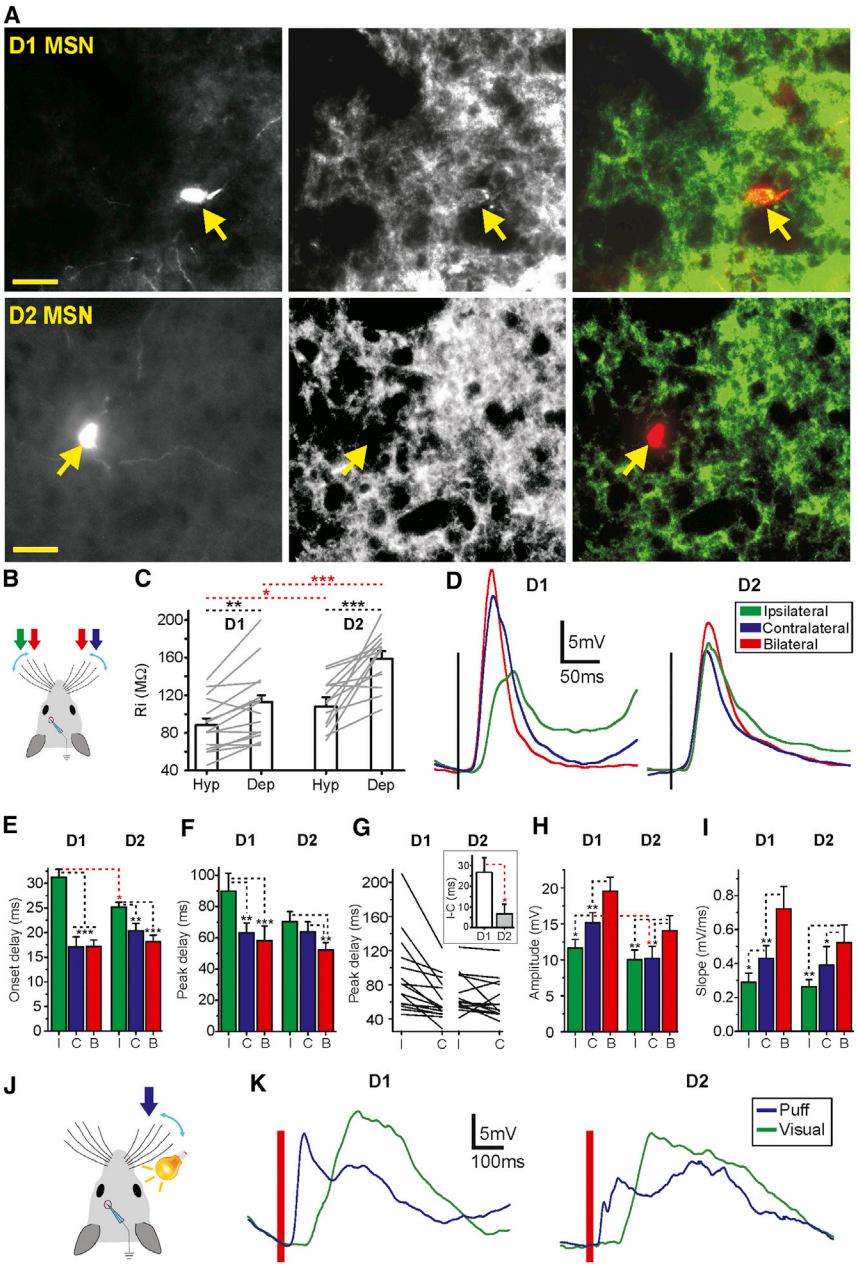

Figure 5. Direct and Indirect Pathway MSNs Respond Differently to Bilateral Whisker Deflection

(A) Examples of immunohistochemistry for identifying D1 and putative D2 MSNs. From left to right; Neurons filled with neurobiotin, D1 receptor expression, and merged images of neurobiotin (red) and D1 receptor expression (green). Yellow narrows indicate the corresponding neuron position in the respective images.

(B) A schematic of the whisker stimulation procedure.

(C) Input resistance for D1 and D2 MSNs calculated from voltage responses to hyperpolarizing and depolarizing current steps during down states.

(D) Waveform averages of responses to whisker deflections in D1 MSN (left) and D2 MSN (right).

(E, F, H, and I) Averages comparing the responses for contralateral (blue), ipsilateral (green), and bilateral stimulation (red) in D1 and D2 MSNs during down states (D1 MSN n = 15; D2 MSN n = 13). Average onset delays (E), peak delays (F), amplitudes (H), and slopes (I).

(G) Peak delays for all D1 and D2 subpopulations in response to contralateral and ipsilateral stimuli. Inset shows the time difference between the peak of the ipsilateral and contralateral responses for D1 and D2 MSNs.

(J) A schematic of the contralateral whisker and visual stimulation protocol.

(K) Examples of average responses to whisker and visual stimulation in D1 (left) and D2 (right) MSNs.

Error bars represent the SEM and asterisks *, **, and *** represent p values smaller than 0.05, 0.01, and 0.001, respectively.

the fastest slopes for bilateral stimulation (see Table 2; Figure 5I). Differences between D1 and D2 MSNs in their responses to whisker stimulation persisted also when occurring during UP states (Figure S6); however, no differences were observed in spontaneous UP states amplitudes or durations (Vm down states D1 −72.28 ± 5.44 mV, D2 −72.66 ± 3.02 mV; AP threshold D1 −46.24 ± 3.31 mV, D2 −45.71 ± 3.73 mV; UP state amplitude D1 11.41 ± 3.16 mV, D2 12.24 ± 4.6 mV; Up state duration D1 0.62 ± 0.18 s, D2 0.61 ± 0.26 s; AP frequency D1 0.16 ± 0.31 Hz, D2 0.10 ± 0.13 Hz) (Figure S6). We also recorded from identified MSNs in dorsomedial striatum that responded to whisker and visual stimulation (five D1-MSNs and three D2-MSNs), thus showing that both MSN types integrate multimodal sensory inputs (Figures 5, 5J, and 5K). The small sample size of type-identified visually responding MSNs prevents us from drawing conclusions regarding their respective integration properties.

In summary, MSNs belonging to the direct and indirect pathways exhibited significant differences in their bilateral integration of tactile sensory inputs. Direct pathway MSNs (D1) responded earlier (onset delay), stronger (amplitude), and faster (slope) to contralateral compared to ipsilateral whisker stimulation. In contrast, in D2 MSNs contralateral and ipsilateral stimulation resulted in more similar response properties, with ipsilateral responses being earlier (onset) and faster (slope). These results suggest that D1 and D2 MSNs have different roles in their sensory integration, D1 MSNs tuned to detect differences between ipsilateral and contralateral whiskers than D2 MSNs, which act as integrators of bilateral inputs.

Sensory Integration by Striatal Interneurons

Striatal interneurons form a small albeit diverse minority in the striatal microcircuitry; therefore, our method of "blind" whole-cell patch-clamping resulted in a rather small number of

Table 2. Responses to Bilateral Whisker Stimulation Recorded in Direct and Indirect Pathway MSNs

	Ipsi		Contra		Both	
	Up	Down	Up	Down	Up	Down
Onset (ms)						
D1	31.07 ± 10.88	31.18 ± 6.49	14.97 ± 6.02	17.07 ± 7.97	16.48 ± 4.83	17.13 ± 5.14
D2	25.15 ± 11.1	25.16 ± 3.68	19.71 ± 7.98	20.38 ± 5.34	15.77 ± 10.93	18.12 ± 4.79
Peak (ms)						
D1	74.49 ± 31.94	89.85 ± 44.44	49.63 ± 27.89	63.08 ± 24.87	50.6 ± 30	58.18 ± 35.05
D2	49.2 ± 10.82	70.33 ± 23.47	44.93 ± 15.51	63.71 ± 23.51	38.37 ± 10.62	52.30 ± 16.78
Amplitude (mV)						
D1	4.01 ± 3.4	11.62 ± 4.68	7.73 ± 5.89	15.15 ± 5.48	12.94 ± 5.81	19.53 ± 7.33
D2	3.1 ± 2.49	10 ± 4.93	3.47 ± 2.77	10.17 ± 6.2	4.92 ± 3.6	14.02 ± 7.58
Normalized amplitude						
D1	0.29 ± 0.16	0.82 ± 0.33	0.48 ± 0.3	1 ± 0	0.53 ± 0.17	1.3 ± 0.42
D2	0.32 ± 0.25	1.13 ± 0.5	0.35 ± 0.25	1 ± 0	0.38 ± 0.28	1.42 ± 0.37
Slope (mV/ms)						
D1	0.13 ± 0.1	0.29 ± 0.2	0.3 ± 0.25	0.43 ± 0.29	0.33 ± 0.22	0.72 ± 0.5
D2	0.16 ± 0.06	0.26 ± 0.15	0.21 ± 0.13	0.39 ± 0.39	0.27 ± 0.12	0.52 ± 0.37

Mean values ± SD. The normalization was done with respect to the contralateral average amplitude during down states for each neuron.

interneurons. Out of 109 recorded striatal neurons, four were classified as interneurons, of which two were fast spiking (Figures S7A–S7D) and two others were cholinergic interneurons (Figures S7E–S7H). Neurons were initially classified according to their recorded electrical properties and following morphological staining, according to the aspiny dendrites and the large soma size (in the case of the cholinergic interneurons). FS interneurons displayed narrow action potentials, relatively depolarized rest potential, high discharge rate of action potentials during UP states, and no apparent inward rectification. Cholinergic interneurons were characterized by their voltage sag response to current step injections, depolarized membrane potential, and spontaneous discharge activity. They also displayed spontaneous slow wave activity, although the amplitude range was not as wide as in FS interneurons or MSNs yet was sufficient to phase-lock spontaneous discharge to the cortical oscillations as recorded simultaneously in S1 and V1 (Figure S7). As in all other recorded neurons, interneurons responded to either whisker stimulation with stronger and earlier responses to the contralateral whisker deflection (Figures S7C, S7G, and S7I), and in one interneuron where visual responses were tested, the recorded FS responded to visual input (Figure S7C).

DISCUSSION

In this study we used whole-cell patch-clamp recordings to study the integration of bilateral and multimodal sensory information in striatal neurons. We show that individual striatal neurons integrate bilateral as well as multisensory inputs, that both spontaneous and sensory evoked inputs are comprised of overlapping excitatory and inhibitory synaptic input, and that MSNs of the direct and indirect pathways differ in the way they integrate bilateral sensory input. All neurons recorded in dorsal striatum, including projection neurons and interneurons, responded to bilateral whisker stimulation in a type-dependent manner, and a population of dorsomedial neurons also responded to visual input. Recordings were obtained under anesthesia, enabling activation of sensory pathways while avoiding interference with motor related inputs. In future studies it would be of interest to study these sensorimotor interactions in the unanesthetized, behaving animal.

Striatal Integration of Bilateral Somatosensory Input

All neurons recorded in the dorsal striatum responded to stimulation of whiskers of both sides. The responses differed in latency, slope, and amplitude, with contralateral whisker stimulation inducing larger and earlier responses as seen also in the recordings from cortical neurons. There are, however, notable differences between the striatal and cortical responses, suggesting different integration properties. Onset delays for contralateral and bilateral responses in dorsolateral MSNs were 6 to 7 ms longer than the cortical ones (Figure 1F). This result, together with the anatomical tracing data, supports the idea that the responses in striatal neurons under our experimental conditions are generated primarily by cortical inputs without engaging a thalamic shortcut (Mowery et al., 2011). Bilateral responses were relatively larger in striatal neurons than in cortical ones (Figure 1H), showing that striatal MSNs act as integrators of bilateral sensory input to a higher degree than cortical neurons. This result can be explained by the time differences between ipsilateral and contralateral onset latencies, which were shorter in striatal neurons, in particular D2 MSNs (Figure 5G, inset). The sensory responses we observed were almost entirely subthreshold, compared to a larger fraction of suprathreshold responses to contralateral whisker stimulation recently reported in rats (Pidoux et al., 2011). The discrepancy in the measured contralateral responses may be explained by differences in the air puff duration and pressure settings (see Experimental

Procedures), striatal coordinates (medial-lateral or rostro-caudal axes), and species (rat and mouse), but it may also be attributed to differences between intracellular sharp and whole-cell recordings (Staley et al., 1992).

Neurons in both dorsolateral and dorsomedial striatum responded to bilateral whisker stimulation; however, these responses differed in several aspects. Response amplitudes and slopes were larger in dorsolateral striatum (Figures 4F–4I); however, onset latencies were similar between the two regions, suggesting that both receive monosynaptic inputs from S1. These results together with the anatomical results (Figure 1B) suggest that the primary target receiving whisker information is indeed the dorsolateral striatum. A larger striatal area, however, receives the sensory input generating an attenuated and slower response, which, in the case of the dorsomedial striatum, also receives sensory information from a different modality (Figures 4A–4E). These differences in sensory input to dorsolateral and dorsomedial striatal regions may underlie the differences in their discharge pattern as recorded during task performance (Thorn et al., 2010).

Sensory-evoked responses in striatal neurons in all tested cases were composed of excitatory and inhibitory components (Figure 2). Inhibition followed excitation by a few milliseconds, suggesting that it was mediated by intrastriatal GABAergic neurons driven by the same excitatory input. Although the inhibitory component was smaller in amplitude than the excitatory input, it could be strong enough to shape striatal output by preventing or delaying MSN discharge (Koós and Tepper, 1999). In vivo studies in neocortex have shown that visual and tactile sensory input induces temporally complex inhibitory inputs mediated by GABAergic interneurons (Haider et al., 2013; Monier et al., 2003; Okun and Lampl, 2008). Whereas in neocortical circuits inhibition is mediated by GABAergic interneurons, in the striatum at least part of the inhibitory component may arise from MSN collaterals (Tunstall et al., 2002), in addition to that from GABAergic interneurons. It is not known which interneurons provide the observed inhibition onto MSNs; however, likely candidates are parvalbumin-expressing FS interneurons (Gerfen et al., 1985). FS interneurons provide robust perisomatic inhibition to MSNs (Gittis et al., 2010; Koós and Tepper, 1999; Planert et al., 2010) and are the first neurons to be activated by cortical input, even before neighboring MSNs (Mallet et al., 2005). A similar form of feedforward inhibition from FS interneurons onto projection neurons exists in the thalamocortical pathway, where an early activation of FS interneurons by thalamic synaptic input provides rapid disynaptic inhibition of excitatory neurons (Cruikshank et al., 2007). Inhibition was also present during ongoing activity, in particular during up states (Figures 2A and S4), as reported also in cortical up states (Haider et al., 2006; Okun and Lampl, 2008). This form of inhibition is likely to originate from striatal neurons that are active during up states; however, the identity of these neurons is not clear. In our recordings, only a small fraction of MSNs discharged spontaneous action potentials, whereas the small sample of recorded FS interneurons were more spontaneously active (Figure S7). Striatal inhibition may also arise from external sources such as neurons in *globus pallidus*, which increase their discharge rate during striatal up states (Goldberg et al., 2003). A particularly robust pallidostriatal inhibitory pathway is mediated by the recently described *arkypallidal* neurons (Mallet et al., 2012). The source of inhibition during both spontaneous activity and sensory-evoked responses should be addressed in future studies using cell-type-specific manipulations.

Multisensory Integration

Visual responses were seen in neurons recorded in the dorsomedial striatum in a relatively large yet restricted striatal region that also received axonal projections from visual cortex, thus suggesting that at least part of the response was mediated by excitatory projections from visual cortex (Figure 3). Visually evoked responses were recently described in neurons from rat dorsal striatum, mediated mainly by subcortical inputs following disinhibition of superior colliculus (Schulz et al., 2011; Schulz et al., 2009). In those studies, visual responses were sparse under control conditions and were significantly enhanced following disinhibition. Recorded neurons were located more laterally than in the present study, which together with the different species and anesthesia may explain the different visual responsiveness. As in the current study, responses were almost entirely subthreshold and had similar latencies (Schulz et al., 2009), suggesting that the visual responses in our recordings may originate from multiple afferent pathways, both cortical and subcortical.

Multisensory responses have been described in different basal ganglia nuclei including the striatum using intracellular, extracellular, and optical recordings (Chudler et al., 1995; Cui et al., 2013; Hikosaka et al., 1989; Nagy et al., 2005, 2006; Wilson et al., 1983). Those studies show that a fraction of striatal neurons changed their discharge rate when presented with sensory input of different modalities, mainly somatosensory and auditory. Our findings support these studies and describe the synaptic input underlying such cross modal interactions. The striatal neurons we recorded in dorsal striatum showed clear preference for whisker stimulation, while only a fraction of them responded to both tactile and visual input, depending on their topographic location (Figure 4C).

Responses to whisker stimulation were significantly earlier than those to visual stimulation (Figure 4). In the neocortex, whisker responses also show shorter latencies (Manns et al., 2004) compared to responses to visual stimulation (Porciatti et al., 1999; Takagaki et al., 2008). The longer latencies in visual responses are in part attributed to retinal processing and may functionally be compensated via retinal motion prediction (Berry et al., 1999). Another possible explanation may lie in the nature of these stimuli, with tactile stimulation originating from nearby objects, whereas visual input would originate from more distal objects, before touching the whiskers. These differences in processing time between visual and tactile stimuli suggest that introducing a time lag between tactile and visual stimuli would result in increased responsiveness in the striatum, as observed in cortical multisensory areas (Olcese et al., 2013). In agreement with the cortical studies, we showed that maximal response amplitude occurred when visual and whisker inputs simultaneously impinged onto postsynaptic MSNs.

In the current study we only studied visual and tactile sensory integration; however, the striatum also integrates other sensory modalities such as auditory (Bordi and LeDoux, 1992) and

olfactory (McDonald, 1991; Novejarque et al., 2011) inputs. In this study we obtained recordings under anesthesia, enabling the selective activation of sensory pathways, without ''contamination'' by motor related interactions.

Further research addressing multisensory information should also consider other sensory modalities as well as the effects of anesthesia, brain-state, and motor activity on sensory integration (Haider et al., 2013; Polack et al., 2013).

Neuron-Subtype-Dependent Sensory Integration

We recorded from several neuronal subtypes and observed differences in their spontaneous activity and response to sensory stimuli. Differences in input resistance between direct and indirect pathway MSNs have been observed in slices (Gertler et al., 2008; Planert et al., 2013). We found similar results in vivo, showing higher input resistance in D2 MSNs, which supports the higher excitability and activity rate of this subpopulation (Cui et al., 2013; Kravitz et al., 2010).

Bilateral cortical input has been reported for both direct and indirect pathway MSNs; however, there is a debate regarding the bias in target preference for the different cell types (Kress et al., 2013; Lei et al., 2004; Reiner et al., 2010; Wall et al., 2013). The difference we observed in the bilateral integration between D1 and D2 MSNs may reflect differences between the afferent corticostriatal pathways to the two populations. In this case, our results would support the findings describing ipsilateral as well as contralateral corticostriatal projection onto both D1 and D2 MSNs and a stronger ipsilateral corticostriatal projection to D1 than D2 MSNs (Kress et al., 2013). Another explanation may lay in the intrinsic properties of MSNs subpopulations, in particular the increased excitability of D2 MSNs and their calcium-mediated dendritic depolarization, which were shown to be different from D1 MSNs (Day et al., 2008).

We also recorded from a small number of FS and cholinergic interneurons. Although our data set is too small to enable a quantitative characterization, a few observations are important to note. All interneurons displayed the slow wave oscillations as was the case for MSNs and cortical pyramidal cells. As seen in Figures S4 and S7, interneurons differed in the oscillation amplitudes and shape, suggesting different connectivity patterns conveying the afferent inputs to these neurons. All interneurons responded to bilateral whisker stimulation, and in a single FS interneuron tested for visual stimulation, such responses were indeed observed, showing that FS interneurons as well as MSNs perform multisensory integration. Further studies should elucidate the functional role of the different interneuron types in sensory integration using the large and growing arsenal of molecular tools (Fenno et al., 2011).

EXPERIMENTAL PROCEDURES

Ethical Approval

All experiments were performed according to the guidelines of the Stockholm municipal committee for animal experiments.

Electrophysiological Recordings

Adult C57BL6 mice of both sexes between 2 and 6 months of age were used to perform the experiments (n = 92). Anesthesia was induced by intraperitoneal injection of ketamine (75 mg/kg) and medetomidine (1 mg/kg) diluted in 0.9% NaCl. Temperature was maintained between 36°C–37.5°C using a feedback-controlled heating pad (FHC Inc.). Craniotomies were made at five sites for patch-clamp and extracellular recordings: AP 0 mm from Bregma, L 2.5 mm (dorsomedial striatum); AP 0 mm from Bregma, L 3.75 mm (dorsolateral striatum); AP −1.5 mm, L 3.25 mm (S1); AP 1.5 mm, L 2.0 mm (M1); AP −3.5 mm, L 2.5 mm (V1) (following Paxinos and Franklin, 2001).

Whole-Cell Recordings

Whole-cell recordings were obtained from dorsolateral striatum between 1,854–2,613 μm deep and in layer V of cortical barrel field between 617–863 μm from the pia, in a perpendicular penetration angle. Signals were amplified using MultiClamp 700B amplifier (Molecular Devices) and digitized at 20 kHz with a CED acquisition board and Spike 2 software (Cambridge Electronic Design). Patch pipettes were pulled with a Flaming/Brown micropipette puller P-87 (Sutter Instruments) and had an initial resistance of 5–12 MΩ.

Extracellular Recordings

Extracellular recordings were obtained using tungsten electrodes with impedances of 1 to 2 MΩ. The electrodes were placed in infragranular layers in somatosensory (BF), motor (M1), and visual (V1) cortex with an angle between 15° and 25°. Recordings were amplified using a Differential AC Amplifier model 1700 (A-M Systems) and digitized at 20 KHz with CED and Spike-2 simultaneously with the whole-cell recording.

Stimulation Protocols

Whisker Stimulation

Whisker stimulation was obtained by brief air puffs delivered by a picospritzer unit (Picospritzer III, Parker Hannifin) via 1 mm diameter plastic tubes placed at ~20 mm in front of the whiskers of both sides. Air puffs (15 ms duration) were given at least 40 times for each stimulus condition (ipsilateral, contralateral, or bilateral stimulation) in a random order, with 5 s of interstimulus interval.

Visual Stimulation

Visual stimulation was delivered by a white LED positioned 50 mm from the contralateral eye. Stimulus duration was 10 ms and was delivered with interstimulus intervals of at least 5 s. The eye was covered with Vaseline in order to prevent drying, as previously described (Holtmaat et al., 2009). Visual responses were confirmed by monitoring the activation of the contralateral visual cortex using extracellular recordings (Figure 3).

Anatomy

Anterograde Tracing

Tracer injections were made using glass pipettes (borosilicate, OD = 1.5 mm, ID = 1.18 mm) with a tip diameter of 5–10 μm. A total of 150–250 nl of BDA 10% (10,000 MW lysine-fixable biotin dextran amine, Molecular Probes) was dissolved in 0.9% NaCl and fast green (to aid visualization of the injected tracer). Injections were performed in layer 5 of BF and V1 using air pressure pulses. A single injection was done for each cortical area and animal using the coordinates described above, as taken from Paxinos and Franklin (2001). Three to six days following injections, animals were transcardially perfused with a solution containing 4% formalin and 14% saturated picric acid dissolved in 0.1 M phosphate buffer (PB) (pH 7.4). Coronal slices (20 μm thick) of both hemispheres containing the entire striatum (from AP 1.7 mm to AP −2.3 mm, following Paxinos and Franklin, 2001) were obtained using a cryostat and collected on gelatin-coated slides. Sections were incubated over night with Cy3-conjugated streptavidin (Jackson ImmunoResearch Laboratories) and NeuroTrace 500/525 Green Fluorescent Nissl Stain (Invitrogen) diluted (1:1,000) in 1% BSA, 0.3% Triton X-100 in 0.1 M PB.

Morphological Staining

At the end of each electrophysiological experiment the mouse was perfused and the brain was placed in fixative solution for 1 to 2 hr in order to stain the neurobiotin-filled neurons (same procedures and solution described above). Sections (10–12 μm thick) mounted on gelatin-coated slides were incubated overnight with Cy2-conjugated streptavidin (Jackson ImmunoResearch Laboratories) diluted (1:500) in 1% BSA, 0.3% Triton X-100 in 0.1 M PB. In between all experimental procedures, slices were washed with 0.01 M PBS. We used fluorescent microscopy to find stained neurons. The shortest recording duration for a stained neuron was 24 min, and the average was 55.44 ± 17.87 min (n = 45). Neurons were then reconstructed using a confocal microscope (Zeiss LSM 510 Meta).

Immunohistochemistry

Reconstructed striatal neurons were immunolabeled for the detection of D1 dopamine receptors, where we found MSNs that clearly expressed D1 or not (D1 n = 15; D2 n = 13). Primary and secondary antibodies were diluted in 1% BSA, 0.3% Triton X-100 in 0.01 M PBS. We used fluorescent and confocal microscopy to recognize the MSN receptor expression (D1). In order to control for the efficacy of the D1 receptor expression described above, we stained slices from D2 EGFP mice, showing that D2 expressing neurons were not stained by the antibody (Figure S5).

SUPPLEMENTAL INFORMATION

Supplemental Information includes seven figures, and Supplemental Experimental Procedures and can be found with this article online at http://dx.doi.org/10.1016/j.neuron.2014.07.033.

ACKNOWLEDGMENTS

We thank Abdel El Manira, Ilan Lampl, Henrik Jörntell, and Maya Ketzef for comments on early versions of the manuscript. This work was supported by the following grants to G.S.: an ERC starting grant, the Knut and Alice Wallenberg Academy Fellowship, the Karolinska Institutet Strategic Research program in Neuroscience (StratNeuro), and the Swedish Medical Research Council.

Accepted: July 21, 2014
Published: August 21, 2014

REFERENCES

Adler, A., Katabi, S., Finkes, I., Israel, Z., Prut, Y., and Bergman, H. (2012). Temporal convergence of dynamic cell assemblies in the striato-pallidal network. J. Neurosci. *32*, 2473–2484.

Albin, R.L., Young, A.B., and Penney, J.B. (1989). The functional anatomy of basal ganglia disorders. Trends Neurosci. *12*, 366–375.

Alexander, G.E., and Crutcher, M.D. (1990). Functional architecture of basal ganglia circuits: neural substrates of parallel processing. Trends Neurosci. *13*, 266–271.

Alloway, K.D., Crist, J., Mutic, J.J., and Roy, S.A. (1999). Corticostriatal projections from rat barrel cortex have an anisotropic organization that correlates with vibrissal whisking behavior. J. Neurosci. *19*, 10908–10922.

Alloway, K.D., Lou, L., Nwabueze-Ogbo, F., and Chakrabarti, S. (2006). Topography of cortical projections to the dorsolateral neostriatum in rats: multiple overlapping sensorimotor pathways. J. Comp. Neurol. *499*, 33–48.

Alloway, K.D., Smith, J.B., Beauchemin, K.J., and Olson, M.L. (2009). Bilateral projections from rat MI whisker cortex to the neostriatum, thalamus, and claustrum: forebrain circuits for modulating whisking behavior. J. Comp. Neurol. *515*, 548–564.

Berke, J.D., Okatan, M., Skurski, J., and Eichenbaum, H.B. (2004). Oscillatory entrainment of striatal neurons in freely moving rats. Neuron *43*, 883–896.

Berry, M.J., 2nd, Brivanlou, I.H., Jordan, T.A., and Meister, M. (1999). Anticipation of moving stimuli by the retina. Nature *398*, 334–338.

Bordi, F., and LeDoux, J. (1992). Sensory tuning beyond the sensory system: an initial analysis of auditory response properties of neurons in the lateral amygdaloid nucleus and overlying areas of the striatum. J. Neurosci. *12*, 2493–2503.

Brown, L.L., Hand, P.J., and Divac, I. (1996). Representation of a single vibrissa in the rat neostriatum: peaks of energy metabolism reveal a distributed functional module. Neuroscience *75*, 717–728.

Calabresi, P., Pisani, A., Mercuri, N.B., and Bernardi, G. (1996). The corticostriatal projection: from synaptic plasticity to dysfunctions of the basal ganglia. Trends Neurosci. *19*, 19–24.

Carman, J.B., Cowan, W.M., Powell, T.P., and Webster, K.E. (1965). A Bilateral Cortico-Striate Projection. J. Neurol. Neurosurg. Psychiatry *28*, 71–77.

Chudler, E.H., Sugiyama, K., and Dong, W.K. (1995). Multisensory convergence and integration in the neostriatum and globus pallidus of the rat. Brain Res. *674*, 33–45.

Cruikshank, S.J., Lewis, T.J., and Connors, B.W. (2007). Synaptic basis for intense thalamocortical activation of feedforward inhibitory cells in neocortex. Nat. Neurosci. *10*, 462–468.

Cui, G., Jun, S.B., Jin, X., Pham, M.D., Vogel, S.S., Lovinger, D.M., and Costa, R.M. (2013). Concurrent activation of striatal direct and indirect pathways during action initiation. Nature *494*, 238–242.

Day, M., Wokosin, D., Plotkin, J.L., Tian, X., and Surmeier, D.J. (2008). Differential excitability and modulation of striatal medium spiny neuron dendrites. J. Neurosci. *28*, 11603–11614.

Doig, N.M., Moss, J., and Bolam, J.P. (2010). Cortical and thalamic innervation of direct and indirect pathway medium-sized spiny neurons in mouse striatum. J. Neurosci. *30*, 14610–14618.

Donoghue, J.P., and Herkenham, M. (1986). Neostriatal projections from individual cortical fields conform to histochemically distinct striatal compartments in the rat. Brain Res. *365*, 397–403.

Faull, R.L., Nauta, W.J., and Domesick, V.B. (1986). The visual cortico-striato-nigral pathway in the rat. Neuroscience *19*, 1119–1132.

Fenno, L., Yizhar, O., and Deisseroth, K. (2011). The development and application of optogenetics. Annu. Rev. Neurosci. *34*, 389–412.

Fino, E., and Venance, L. (2011). Spike-timing dependent plasticity in striatal interneurons. Neuropharmacology *60*, 780–788.

Flaherty, A.W., and Graybiel, A.M. (1991). Corticostriatal transformations in the primate somatosensory system. Projections from physiologically mapped body-part representations. J. Neurophysiol. *66*, 1249–1263.

Gerfen, C.R., Baimbridge, K.G., and Miller, J.J. (1985). The neostriatal mosaic: compartmental distribution of calcium-binding protein and parvalbumin in the basal ganglia of the rat and monkey. Proc. Natl. Acad. Sci. USA *82*, 8780–8784.

Gertler, T.S., Chan, C.S., and Surmeier, D.J. (2008). Dichotomous anatomical properties of adult striatal medium spiny neurons. J. Neurosci. *28*, 10814–10824.

Gittis, A.H., Nelson, A.B., Thwin, M.T., Palop, J.J., and Kreitzer, A.C. (2010). Distinct roles of GABAergic interneurons in the regulation of striatal output pathways. J. Neurosci. *30*, 2223–2234.

Goldberg, J.A., Kats, S.S., and Jaeger, D. (2003). Globus pallidus discharge is coincident with striatal activity during global slow wave activity in the rat. J. Neurosci. *23*, 10058–10063.

Haber, S. (2008). Parallel and integrative processing through the Basal Ganglia reward circuit: lessons from addiction. Biol. Psychiatry *64*, 173–174.

Haider, B., Duque, A., Hasenstaub, A.R., and McCormick, D.A. (2006). Neocortical network activity in vivo is generated through a dynamic balance of excitation and inhibition. J. Neurosci. *26*, 4535–4545.

Haider, B., Häusser, M., and Carandini, M. (2013). Inhibition dominates sensory responses in the awake cortex. Nature *493*, 97–100.

Hikosaka, O., Sakamoto, M., and Usui, S. (1989). Functional properties of monkey caudate neurons. II. Visual and auditory responses. J. Neurophysiol. *61*, 799–813.

Holtmaat, A., Bonhoeffer, T., Chow, D.K., Chuckowree, J., De Paola, V., Hofer, S.B., Hübener, M., Keck, T., Knott, G., Lee, W.C., et al. (2009). Long-term, high-resolution imaging in the mouse neocortex through a chronic cranial window. Nat. Protoc. *4*, 1128–1144.

Hoover, J.E., Hoffer, Z.S., and Alloway, K.D. (2003). Projections from primary somatosensory cortex to the neostriatum: the role of somatotopic continuity in corticostriatal convergence. J. Neurophysiol. *89*, 1576–1587.

Kincaid, A.E., and Wilson, C.J. (1996). Corticostriatal innervation of the patch and matrix in the rat neostriatum. J. Comp. Neurol. *374*, 578–592.

Kincaid, A.E., Zheng, T., and Wilson, C.J. (1998). Connectivity and convergence of single corticostriatal axons. J. Neurosci. *18*, 4722–4731.

Kita, T., Kita, H., and Kitai, S.T. (1984). Passive electrical membrane properties of rat neostriatal neurons in an in vitro slice preparation. Brain Res. *300*, 129–139.

Koós, T., and Tepper, J.M. (1999). Inhibitory control of neostriatal projection neurons by GABAergic interneurons. Nat. Neurosci. *2*, 467–472.

Kravitz, A.V., Freeze, B.S., Parker, P.R., Kay, K., Thwin, M.T., Deisseroth, K., and Kreitzer, A.C. (2010). Regulation of parkinsonian motor behaviours by optogenetic control of basal ganglia circuitry. Nature *466*, 622–626.

Kreitzer, A.C., and Malenka, R.C. (2008). Striatal plasticity and basal ganglia circuit function. Neuron *60*, 543–554.

Kress, G.J., Yamawaki, N., Wokosin, D.L., Wickersham, I.R., Shepherd, G.M., and Surmeier, D.J. (2013). Convergent cortical innervation of striatal projection neurons. Nat. Neurosci. *16*, 665–667.

Künzle, H. (1975). Bilateral projections from precentral motor cortex to the putamen and other parts of the basal ganglia. An autoradiographic study in Macaca fascicularis. Brain Res. *88*, 195–209.

Lei, W., Jiao, Y., Del Mar, N., and Reiner, A. (2004). Evidence for differential cortical input to direct pathway versus indirect pathway striatal projection neurons in rats. J. Neurosci. *24*, 8289–8299.

Mallet, N., Le Moine, C., Charpier, S., and Gonon, F. (2005). Feedforward inhibition of projection neurons by fast-spiking GABA interneurons in the rat striatum in vivo. J. Neurosci. *25*, 3857–3869.

Mallet, N., Micklem, B.R., Henny, P., Brown, M.T., Williams, C., Bolam, J.P., Nakamura, K.C., and Magill, P.J. (2012). Dichotomous organization of the external globus pallidus. Neuron *74*, 1075–1086.

Manns, I.D., Sakmann, B., and Brecht, M. (2004). Sub- and suprathreshold receptive field properties of pyramidal neurones in layers 5A and 5B of rat somatosensory barrel cortex. J. Physiol. *556*, 601–622.

McDonald, A.J. (1991). Topographical organization of amygdaloid projections to the caudatoputamen, nucleus accumbens, and related striatal-like areas of the rat brain. Neuroscience *44*, 15–33.

McGeorge, A.J., and Faull, R.L. (1987). The organization and collateralization of corticostriate neurones in the motor and sensory cortex of the rat brain. Brain Res. *423*, 318–324.

Middleton, F.A., and Strick, P.L. (2000). Basal ganglia and cerebellar loops: motor and cognitive circuits. Brain Res. Brain Res. Rev. *31*, 236–250.

Monier, C., Chavane, F., Baudot, P., Graham, L.J., and Frégnac, Y. (2003). Orientation and direction selectivity of synaptic inputs in visual cortical neurons: a diversity of combinations produces spike tuning. Neuron *37*, 663–680.

Mowery, T.M., Harrold, J.B., and Alloway, K.D. (2011). Repeated whisker stimulation evokes invariant neuronal responses in the dorsolateral striatum of anesthetized rats: a potential correlate of sensorimotor habits. J. Neurophysiol. *105*, 2225–2238.

Nagy, A., Paróczy, Z., Norita, M., and Benedek, G. (2005). Multisensory responses and receptive field properties of neurons in the substantia nigra and in the caudate nucleus. Eur. J. Neurosci. *22*, 419–424.

Nagy, A., Eördegh, G., Paróczy, Z., Márkus, Z., and Benedek, G. (2006). Multisensory integration in the basal ganglia. Eur. J. Neurosci. *24*, 917–924.

Niell, C.M., and Stryker, M.P. (2008). Highly selective receptive fields in mouse visual cortex. J. Neurosci. *28*, 7520–7536.

Nisenbaum, E.S., and Wilson, C.J. (1995). Potassium currents responsible for inward and outward rectification in rat neostriatal spiny projection neurons. J. Neurosci. *15*, 4449–4463.

Norita, M., McHaffie, J.G., Shimizu, H., and Stein, B.E. (1991). The corticostriatal and corticotectal projections of the feline lateral suprasylvian cortex demonstrated with anterograde biocytin and retrograde fluorescent techniques. Neurosci. Res. *10*, 149–155.

Novejarque, A., Gutierrez-Castellanos, N., Lanuza, E., and Martinez-Garcia, F. (2011). Amygdaloid projections to the ventral striatum in mice: direct and indirect chemosensory inputs to the brain reward system. Front. Neuroanat. *5*, http://dx.doi.org/10.3389/fnana.2011.00054.

Okun, M., and Lampl, I. (2008). Instantaneous correlation of excitation and inhibition during ongoing and sensory-evoked activities. Nat. Neurosci. *11*, 535–537.

Olcese, U., Iurilli, G., and Medini, P. (2013). Cellular and synaptic architecture of multisensory integration in the mouse neocortex. Neuron *79*, 579–593.

Paxinos, G., and Franklin, K. (2001). The Mouse Brain in Stereotaxic Coordinates, 2nd Edition. (San Diego: Academic Press).

Pidoux, M., Mahon, S., Deniau, J.M., and Charpier, S. (2011). Integration and propagation of somatosensory responses in the corticostriatal pathway: an intracellular study in vivo. J. Physiol. *589*, 263–281.

Planert, H., Szydlowski, S.N., Hjorth, J.J.J., Grillner, S., and Silberberg, G. (2010). Dynamics of synaptic transmission between fast-spiking interneurons and striatal projection neurons of the direct and indirect pathways. J. Neurosci. *30*, 3499–3507.

Planert, H., Berger, T.K., and Silberberg, G. (2013). Membrane properties of striatal direct and indirect pathway neurons in mouse and rat slices and their modulation by dopamine. PLoS ONE *8*, e57054.

Polack, P.O., Friedman, J., and Golshani, P. (2013). Cellular mechanisms of brain state-dependent gain modulation in visual cortex. Nat. Neurosci. *16*, 1331–1339.

Porciatti, V., Pizzorusso, T., and Maffei, L. (1999). The visual physiology of the wild type mouse determined with pattern VEPs. Vision Res. *39*, 3071–3081.

Reig, R., and Sanchez-Vives, M.V. (2007). Synaptic transmission and plasticity in an active cortical network. PLoS ONE *2*, e670.

Reiner, A., Hart, N.M., Lei, W.L., and Deng, Y.P. (2010). Corticostriatal projection neurons - dichotomous types and dichotomous functions. Front. Neuroanat. *4*, http://dx.doi.org/10.3389/fnana.2010.00142.

Schultz, W., Dayan, P., and Montague, P.R. (1997). A neural substrate of prediction and reward. Science *275*, 1593–1599.

Schulz, J.M., Redgrave, P., Mehring, C., Aertsen, A., Clements, K.M., Wickens, J.R., and Reynolds, J.N. (2009). Short-latency activation of striatal spiny neurons via subcortical visual pathways. J. Neurosci. *29*, 6336–6347.

Schulz, J.M., Oswald, M.J., and Reynolds, J.N. (2011). Visual-induced excitation leads to firing pauses in striatal cholinergic interneurons. J. Neurosci. *31*, 11133–11143.

Serizawa, M., McHaffie, J.G., Hoshino, K., and Norita, M. (1994). Corticostriatal and corticotectal projections from visual cortical areas 17, 18 and 18a in the pigmented rat. Arch. Histol. Cytol. *57*, 493–507.

Smith, Y., Bevan, M.D., Shink, E., and Bolam, J.P. (1998). Microcircuitry of the direct and indirect pathways of the basal ganglia. Neuroscience *86*, 353–387.

Staley, K.J., Otis, T.S., and Mody, I. (1992). Membrane properties of dentate gyrus granule cells: comparison of sharp microelectrode and whole-cell recordings. J. Neurophysiol. *67*, 1346–1358.

Surmeier, D.J., Ding, J., Day, M., Wang, Z., and Shen, W. (2007). D1 and D2 dopamine-receptor modulation of striatal glutamatergic signaling in striatal medium spiny neurons. Trends Neurosci. *30*, 228–235.

Takagaki, K., Zhang, C., Wu, J.Y., and Lippert, M.T. (2008). Crossmodal propagation of sensory-evoked and spontaneous activity in the rat neocortex. Neurosci. Lett. *431*, 191–196.

Thorn, C.A., Atallah, H., Howe, M., and Graybiel, A.M. (2010). Differential dynamics of activity changes in dorsolateral and dorsomedial striatal loops during learning. Neuron *66*, 781–795.

Tunstall, M.J., Oorschot, D.E., Kean, A., and Wickens, J.R. (2002). Inhibitory interactions between spiny projection neurons in the rat striatum. J. Neurophysiol. *88*, 1263–1269.

Wall, N.R., De La Parra, M., Callaway, E.M., and Kreitzer, A.C. (2013). Differential innervation of direct- and indirect-pathway striatal projection neurons. Neuron *79*, 347–360.

Wilson, C.J. (1987). Morphology and synaptic connections of crossed corticostriatal neurons in the rat. J. Comp. Neurol. *263*, 567–580.

Wilson, C.J. (1993). The generation of natural firing patterns in neostriatal neurons. Prog. Brain Res. *99*, 277–297.

Wilson, C.J., and Kawaguchi, Y. (1996). The origins of two-state spontaneous membrane potential fluctuations of neostriatal spiny neurons. J. Neurosci. *16*, 2397–2410.

Wilson, J.S., Hull, C.D., and Buchwald, N.A. (1983). Intracellular studies of the convergence of sensory input on caudate neurons of cat. Brain Res. *270*, 197–208.

Wright, A.K., Ramanathan, S., and Arbuthnott, G.W. (2001). Identification of the source of the bilateral projection system from cortex to somatosensory neostriatum and an exploration of its physiological actions. Neuroscience *103*, 87–96.

Neuron, Volume *83*

Supplemental Information

Multisensory Integration in the Mouse Striatum

Ramon Reig and Gilad Silberberg

Supplemental Information includes:

Figures S1-S7

Supplemental Experimental Procedures

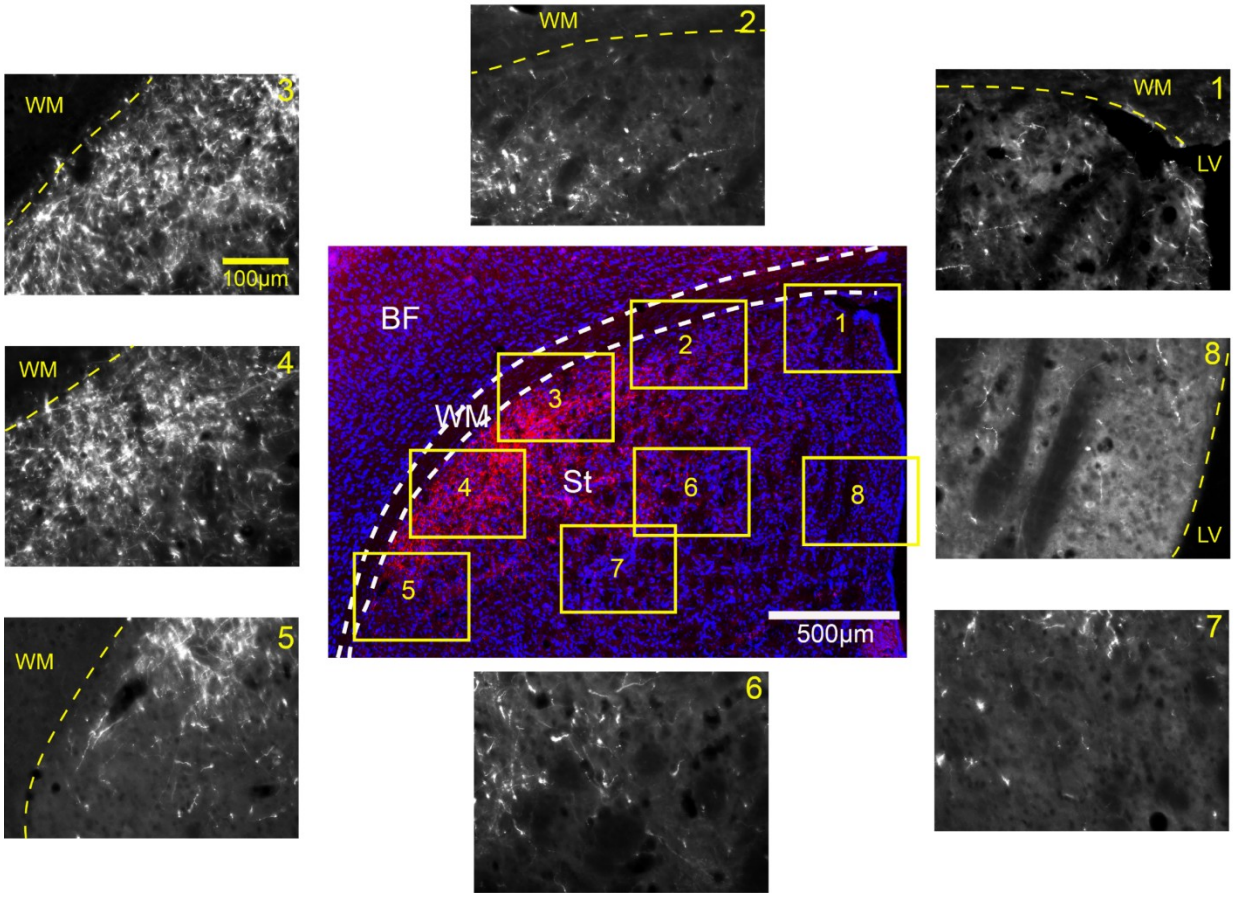

Figure S1. Ipsilateral axonal projections from cortical S1 to dorsal striatum (related to figure 1). Anterograde tracing from layer 5 in cortical S1 (barrel field - BF) to dorsal striatum (center image). Insets 1-8 show higher magnification of axonal projections (in white) throughout dorsal striatum. Note the sparse labeling of cortical axons in dorsomedial striatum (inset 1) compared to the dense labeling in dorsolateral striatum (insets 3-5).

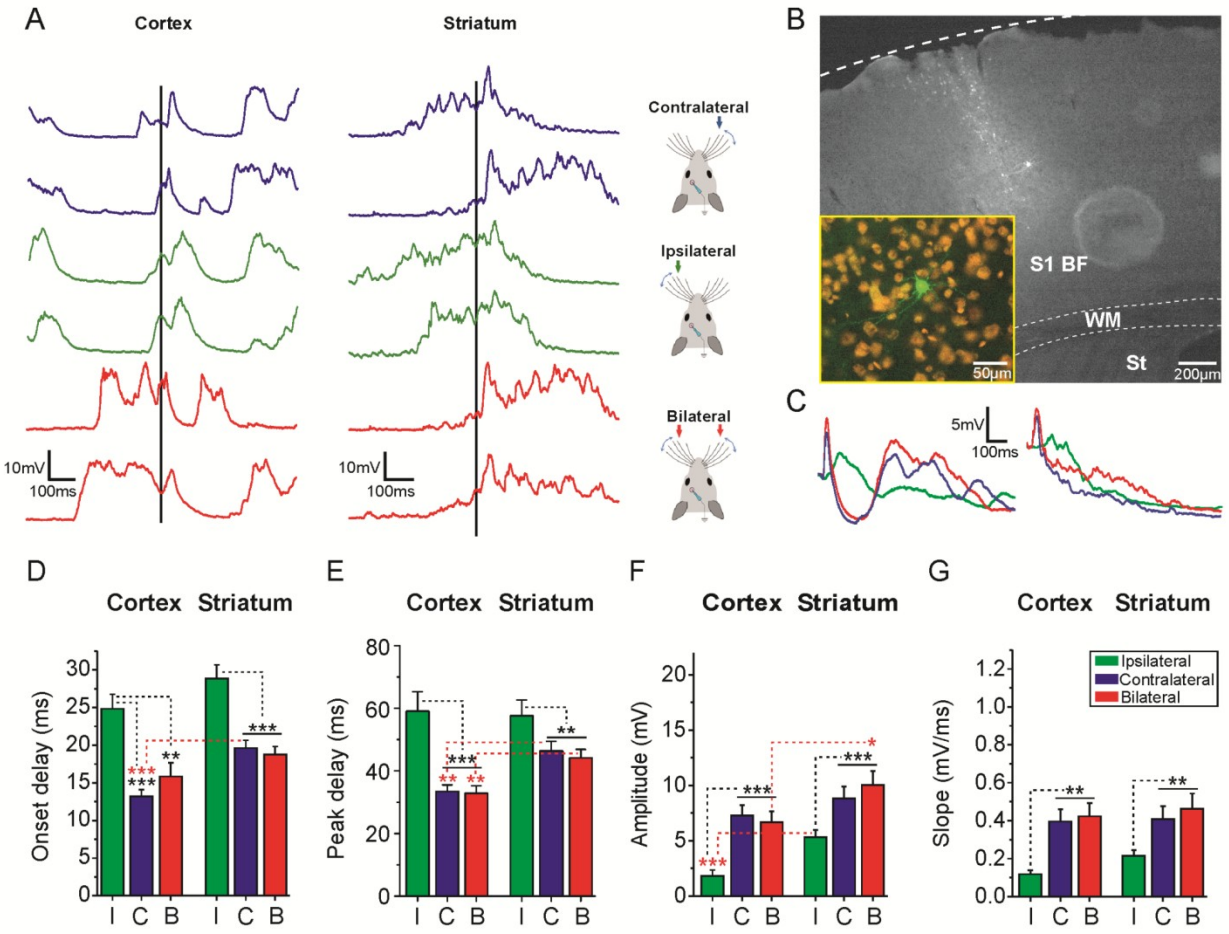

Figure S2. Responses to bilateral whisker deflection in cortical and striatal MSNs during up states (related to Figure 1). A. Example of responses to whisker deflection in a cortical pyramidal neuron (left) and a striatal MSN (right) during up states. **B.** Morphological reconstruction of the pyramidal cortical neuron recorded in A. **C.** Waveform average of the responses for the neurons showed in A. **D-G**. Average responses of cortical and striatal neurons to whisker deflection during up states. Ipsilateral in green, contralateral in blue, and bilateral stimulation in red. Onset delay (D), peak delay (E), amplitude (F), and slope (G). Scales are the same as in Figure 1F-I for comparison of up and down states. Cortical neurons n = 17, striatal MSN n = 20. Error bars represent the standard error of the mean (SEM) and asterisks *, **, *** represent p values smaller than 0.05, 0.01, 0.001, respectively.

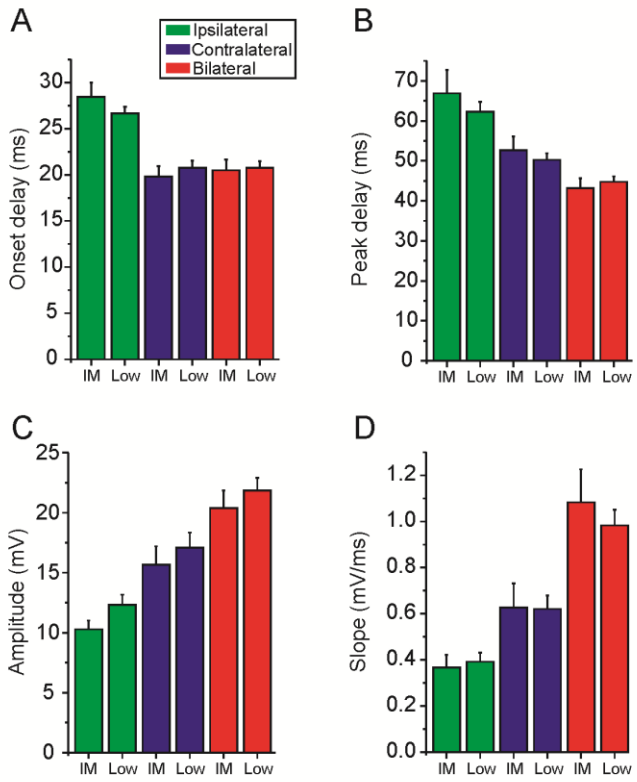

Figure S3. High vs. low chloride intracellular solution in dorsolateral MSNs (related to Figure 2). Average responses of dorsolateral striatal MSNs recorded with Intermediate Cl^- (30 mM, "IM") and Low Cl^- (10 mM, "Low") intracellular solution. Ipsilateral in green, contralateral in blue, and bilateral stimulation in red. Onset delay (A), peak delay (B), amplitude (C), and slope (D). No significant differences were observed between MSNs recorded with intermediate and low chloride solutions, for any of the presented measurements. IM MSNs n = 20, Low MSNs n = 28. Error bars represent the standard error of the mean (SEM).

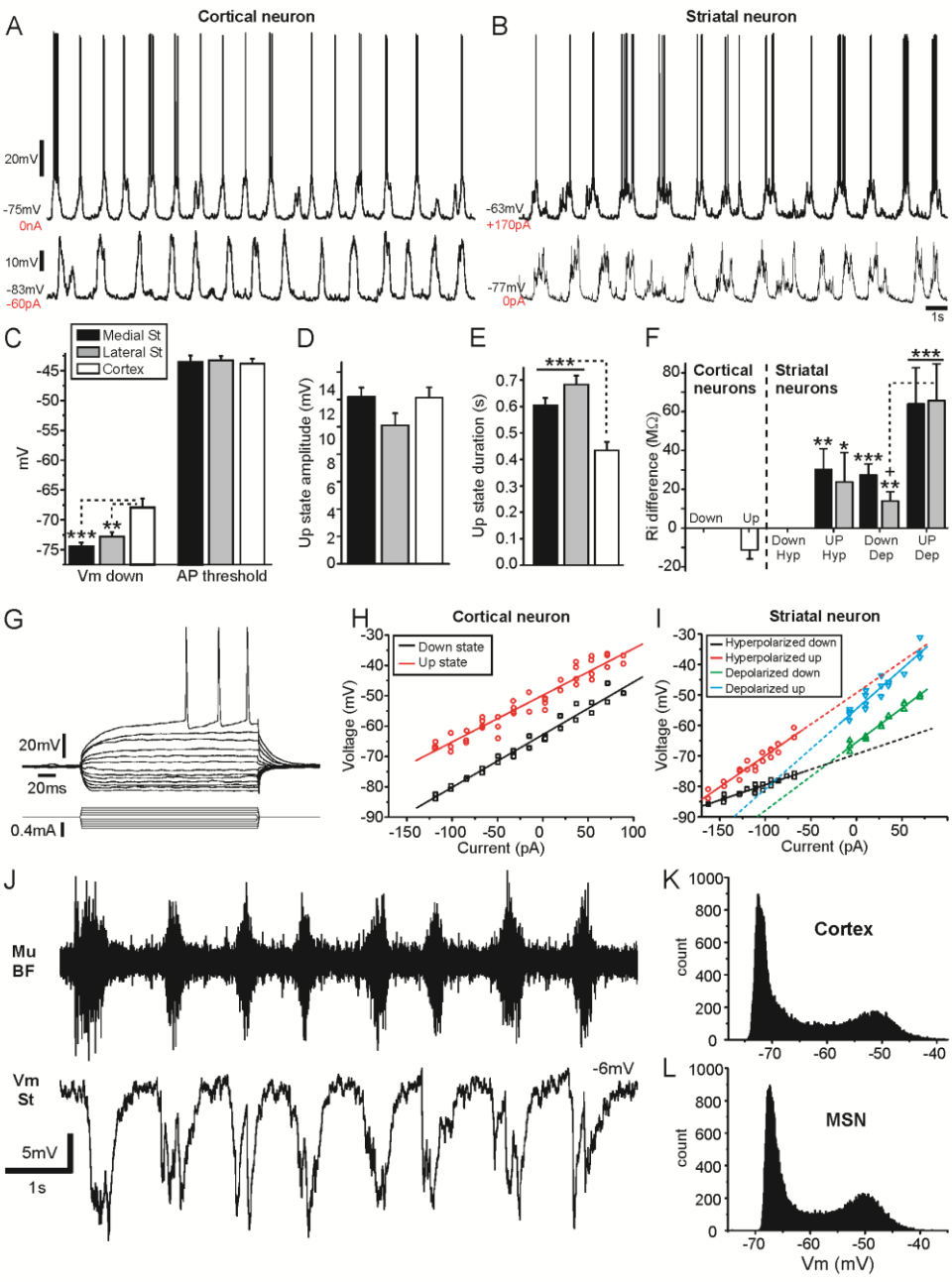

Figure S4. Intrinsic properties and spontaneous activity of cortical and striatal neurons (related to Figures 1 and 2). A-B. Examples of whole-cell patch clamp recordings of spontaneous slow oscillations in cortical and striatal neurons at different holding potentials. Note that at resting membrane potential (0 pA, as shown in red) the cortical but not striatal neuron discharges action potentials during up states. **C-E**. Properties of spontaneous slow oscillations in cortical pyramidal cells and striatal MSNs recorded in dorsomedial (medial St) and dorsolateral (Lateral St). Membrane potential (Vm) during down states and action potential threshold (C). Up state amplitude (D). Up state duration (E). **F**. Changes in the input

resistance of cortical and striatal neurons during up and down states. In MSNs, input resistances were different when extracted from hyperpolarizing and depolarizing current steps due to inward rectification by Kir channels. **G**. Example of current injections steps in a striatal MSN. **H-I**. Examples of current/voltage plots for cortical (H) and striatal (I) neurons, using depolarizing and hyperpolarizing current steps at Down- and UP states. Cortical neurons n = 17, dorsomedial MSNs n = 24, dorsolateral MSNs n = 20. Error bars represent the standard error of the mean (SEM) and asterisks *, **, *** represent p values smaller than 0.05, 0.01, 0.001, respectively. In F, asterisks represent comparison to the "Down Hyperpolarized" condition while "+" represents the comparison with the "UP depolarized" condition. **J.** MSNs receive inhibitory inputs during up states, as seen in the simultaneous extracellular recording in ipsilateral barrel cortex (top trace) and whole-cell recording in a striatal neuron (bottom trace). The recorded neuron was depolarized to the excitatory reversal potential in order to reveal inhibitory voltage responses. **K-L**. Bimodal distribution of membrane potential during spontaneous activity. Examples of bimodal membrane potential distribution of a cortical layer 5 pyramidal neuron (barrel cortex (K)) and a striatal MSN (L).

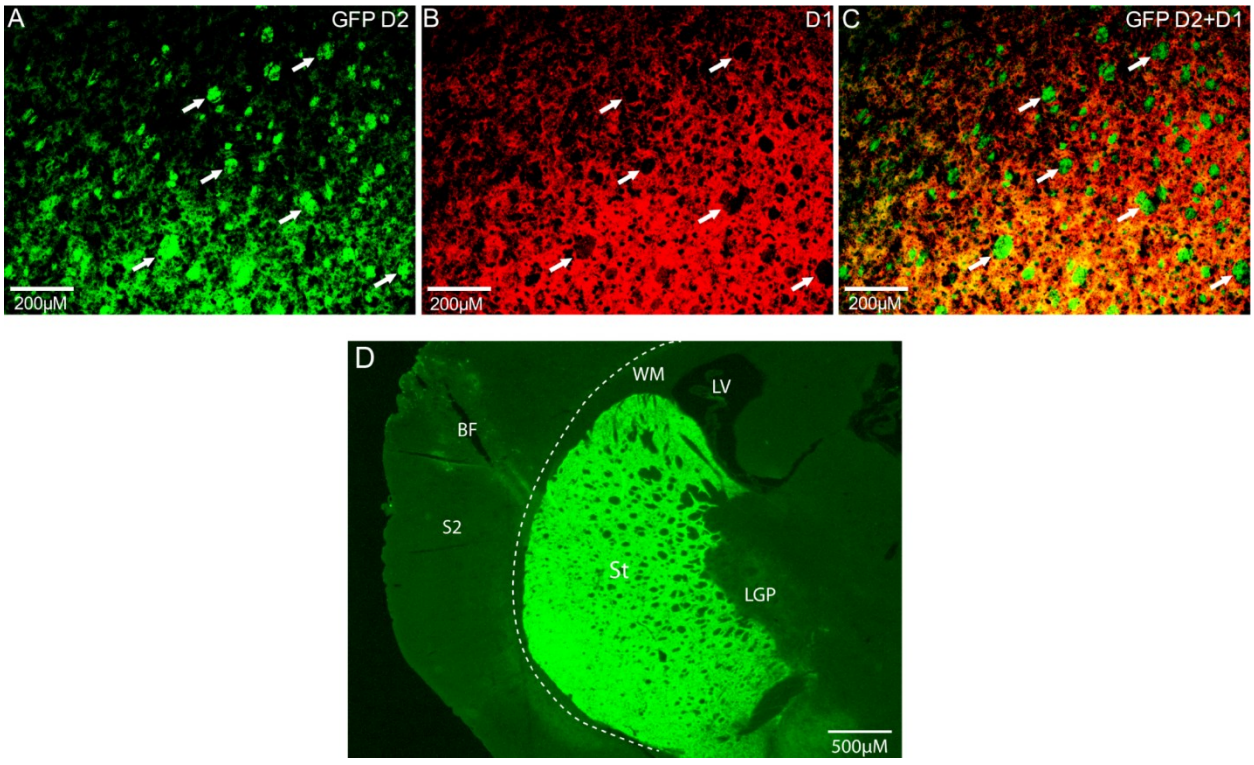

Figure S5. Control experiment showing D1 antibody staining of a slice from a Drd2 BAC transgenic mouse. A-C (related to Figure 5). The arrows point at 6 examples of D2-EGFP positive neurons from a Drd2-BAC transgenic mouse (Gong et al., 2003), all of which are not stained by the D1 antibody, as also evident in the merged image (*right panel*). **D**. Example of D1 inmunostaining in a wild-type mouse, highlighting the strong D1 expression throughout striatum.

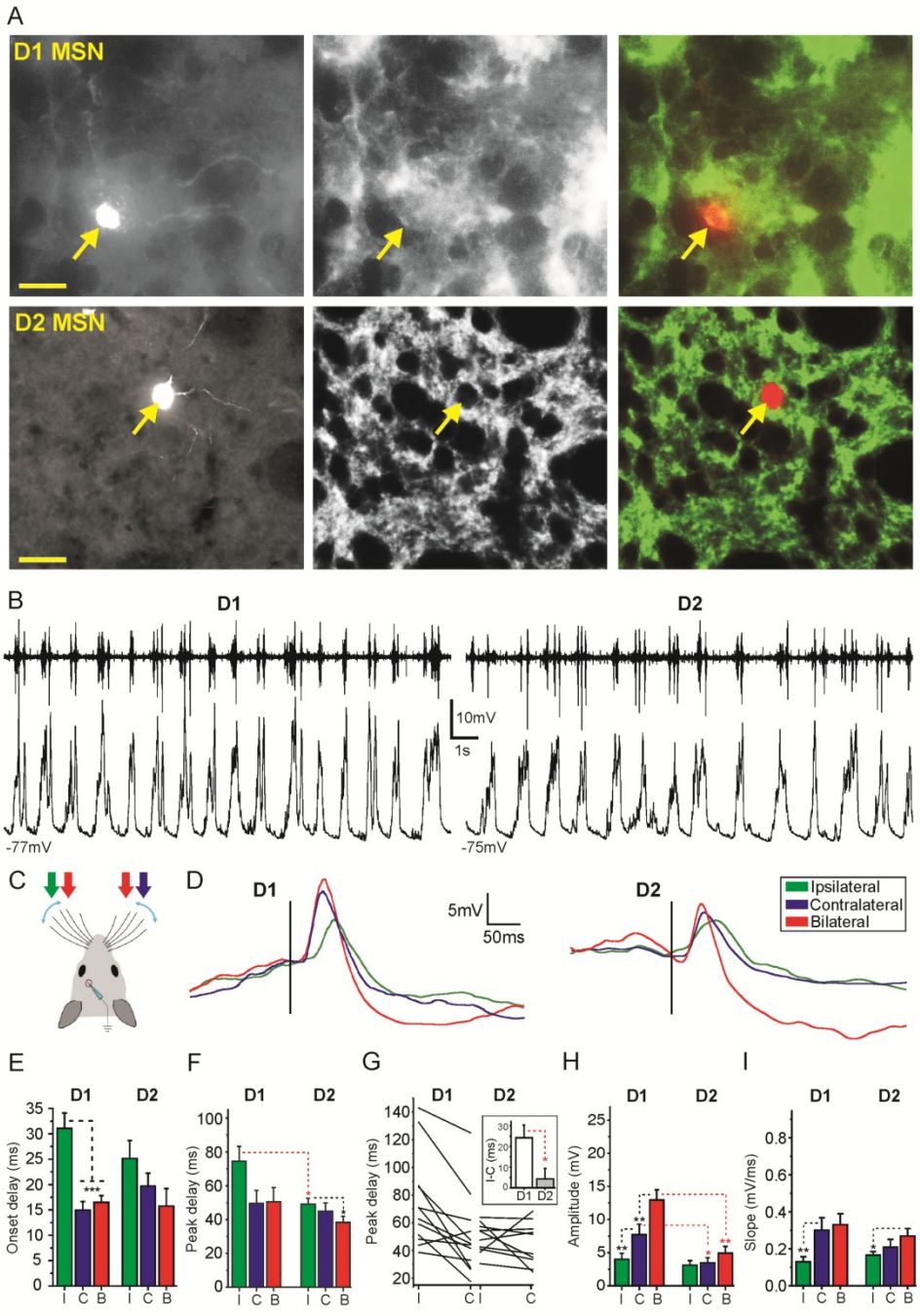

Figure S6. Direct and indirect pathway MSNs responding to bilateral whisker deflection during up states (related to figure 5). A. Examples of inmunohistochemestry for identifying D1 and putative D2 MSNs. From left to right; Neurons filled with neurobiotin, D1 receptor expression, and merged images of neurobiotin (red) and D1 receptor expression (green). Yellow narrows indicate the corresponding neuron position in the respective images **B**. Raw traces of whole cell recordings in D1 (left) and D2 (right) MSNs (bottom traces) and simultaneous extracellular recordings in ipsilateral BF (top traces) during

spontaneous slow oscillations. **C**. A schematic of the whisker stimulation procedure. **D.** Waveform averages of responses to whisker deflections in D1 MSN (left) and D2 MSN (right). **E-F**, **H-I**. Averages comparing the responses for contralateral (blue), ipsilateral (green) and bilateral stimulation (red) in D1 and D2 MSNs during up states. (E) Average onset delays, (F) Peak delays, (I) slopes (D1 MSN = 12; D2 MSN = 10), (H) amplitudes (D1 MSN = 15; D2 MSN = 13, we consider 0mV amplitude when responses were not clear detectable as in the cases of E, F, I, and G). **G**. Peak delays for all D1 and D2 subpopulations in response to contralateral and ipsilateral stimuli. Inset shows the time difference between the peak of the ipsilateral and contralateral responses for D1 and D2 MSNs. Error bars represent the standard error of the mean (SEM) and asterisks *, **, *** represent p values smaller than 0.05, 0.01, 0.001, respectively.

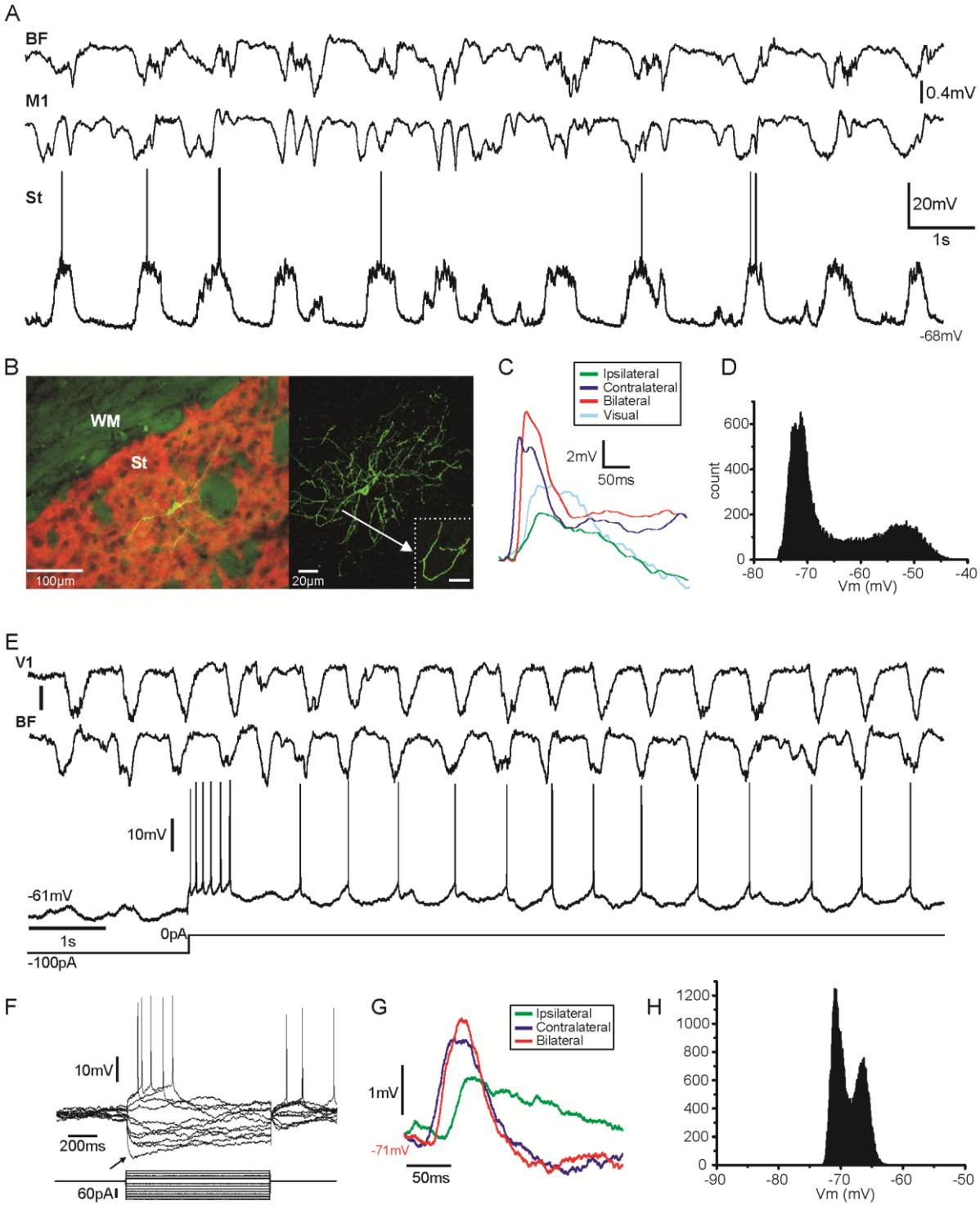

I

	Neuron properties			Onset delay (ms)			Amplitude (mV)			Slope (mV/ms)		
	AP duration (ms)	Vm (mV)	Up states amplitude (mV)	Contra	Ipsi	Bilateral	Contra	Ipsi	Bilateral	Contra	Ipsi	Bilateral
FS1	0.86	-75	15.65	21.15	35.2	31.7	12.35	6.98	14.38	0.73	0.1	0.9
FS2	0.8	-69	11.74	12.86	42.6	9.4	4.65	4.3	7.37	0.12	0.14	0.21
ChI1	1.58	-47.5	6.16	33.2	46.2	34.1	1.8	1.09	2.26	0.074	0.045	0.098
ChI2	1.28	-49.6	5.81	31.7	45.8	30.7	2.49	2.18	2.58	0.067	0.039	0.071

Figure S7. *In vivo* whole cell recordings from striatal interneurons. **A-D. Fast spiking interneuron (related to Figures 2 and 5). A**. An example of simultaneous whole-cell recording from a fast spiking interneuron and dual extracellular recordings in ipsilateral BF and M1 during spontaneous activity. **B**. Fluorescent image (left) and confocal reconstruction (right) of the same interneuron. The inset shows the smooth (aspiny) dendrites. **C**. Waveform average of the interneuron responses to visual stimulation (light blue trace) and ipsilateral (green trace), contralateral (dark blue trace), and bilateral (red trace) whisker deflection. **D**. Bimodal distribution of membrane potential during spontaneous activity. **E-H. Cholinergic interneurons**. **E.** An example of simultaneous whole-cell recording from a cholinergic interneuron and dual extracellular recordings in BF and V1 during spontaneous activity. Note than when the interneuron is not hyperpolarized by negative holding current, it discharges action potentials in synchrony with the cortical up states (negative peaks in the LFP recording). The scale bar for local field potentials is 0.4 mV. **F.** Response of the same cholinergic interneuron to step current injections. Note the voltage sag response (arrow) and rebound spikes characteristic for cholinergic interneurons. **G**. Waveform average of responses to bilateral whisker deflections at hyperpolarized holding potential. **H**. Bimodal distribution of membrane potential during spontaneous activity. **I. Intrinsic properties and responses to bilateral whisker stimulation recorded in striatal interneurons.** Amplitudes of up states and tactile responses were measured at resting membrane potential for FS interneurons and around -70 mV for cholinergic interneurons, during down states.

Experimental Procedures

Ethical approval.

All experiments were performed according to the guidelines of the Stockholm municipal committee for animal experiments.

Electrophysiological recordings.

Adult C57BL6 mice of both sexes between 2-6 months of age were used to perform the experiments (n = 92). Anesthesia was induced by intraperitoneal injection of ketamine (75 mg/kg) and medetomidine (1 mg/kg) diluted in 0.9 % NaCl. A maintaining dose of ketamine (30 mg/kg i.m.) was administrated every 2 hours or after changes in the EEG or reflex responds to paw pinches. Animals were sacrificed after

recordings by receiving an overdose of sodium pentobarbital (200 mg/kg I.P.). Tracheotomy was performed to increase mechanical stability during recordings by decreasing breathing related movements. Mice were placed in a stereotaxic device and air enriched with oxygen was delivered through a thin tube placed 1 cm from the tracheal cannula. Temperature was maintained between 36-37.5 °C using a feedback-controlled heating pad (FHC Inc.). Craniotomies were made at 5 sites for patch clamp and extracellular recordings: AP 0 mm from Bregma, L 2.5 mm (dorsomedial striatum); AP 0 mm from Bregma, L 3.75 mm (dorsolateral striatum); AP -1.5 mm, L 3.25 mm (S1); AP 1.5 mm, L 2 mm (M1); AP -3.5 mm, L 2.5 mm (V1) (following Paxinos and Franklin (2001)).

Whole-cell recordings were obtained from dorsolateral striatum between 1854-2613 µm deep and in layer V of cortical barrel field between 617-863 µm from the pia, in a perpendicular penetration angle (30°-40°). Signals were amplified using MultiClamp 700B amplifier (Molecular Devices) and digitized at 20 KHz with a CED acquisition board and Spike 2 software (Cambridge Electronic Design). Patch pipettes were pulled with a Flaming/Brown micropipette puller P-87 (Sutter Instruments) and had an initial resistance of 5-12 MΩ, with longer tips than the standard ones to minimize cortical damage. Pipettes were back-filled with intracellular solution containing the following (in mM): 125 K-gluconate, 10 KCl, 10 Na-Phosphocreatine, 10 HEPES, 4 ATP-Mg, 0.3 GTP-Na. A subset of experiments was performed with intracellular solution containing 105 K-gluconate, 30 KCl, 10 Na-Phosphocreatine, 10 HEPES, 4 ATP-Mg, 0.3 GTP-Na. Response latencies and amplitudes to whisker stimulation were not different across experiments performed with either intracellular solution (Figure S3).

Extracellular recordings were obtained using tungsten electrodes with impedances of 1-2 MΩ. The electrodes were placed in infragranular layers in somatosensory (BF), motor (M1), and visual (V1) cortex with an angle between 15° and 25°. Recordings were amplified using a Differential AC Amplifier model 1700 (A-M Systems) and digitized at 10 KHz with CED and Spike-2 simultaneously with the whole-cell recording.

Stimulation protocols.

Whisker stimulation was obtained by brief air puffs delivered by a picospritzer unit (Picospritzer III, Parker Hannifin, NJ) via 1 mm diameter plastic tubes placed at ~20 mm in front of the whiskers of both sides. Air puffs (15 ms duration) were given at least 40 times for each stimulus condition (ipsilateral, contralateral, or bilateral stimulation) in a random order, with 5 seconds of inter-stimulus interval. Air pressure was equal in both sides (20 p.s.i.) and evoked synaptic responses when stimulating the

contralateral and ipsilateral whisker. The whisker displacement following air puff was monitored and was determined to occur 11.0 ± 0.1 (n = 3 animals) ms following the trigger command. The reference onset time for the stimulus was therefore determined as 11 ms following the computer trigger command for the air puff.

Visual stimulation was delivered by a white LED positioned 50 mm from the contralateral eye. Stimulus duration was 10 ms and was delivered with interstimulus intervals of at least 5 seconds. The eye was covered with Vaseline in order to prevent drying, as previously described (Holtmaat et al., 2009). Visual responses were confirmed by monitoring the activation of the contralateral visual cortex using extracellular recordings (Figure 3F,G).

Multisensory stimulation. Tactile and visual stimuli were delivered using the same protocols as described above. In a subset of experiment we delivered the whisker stimulation with different delays with respect to the visual stimulus. Specifically, whisker stimulation was delivered in 5 different conditions; 1. Independently, using only contralateral whisker stimulation. 2. Simultaneously triggered with visual stimulation. 3. At the same time as the onset of the visual responses. 4. In synchronization with the peak of the visual response. 5. One second after visual responses. The response onset and peak were obtained independently for each modality and then used in the multisensory stimulation protocols.

Analysis.

Up and Down states were extracted from membrane potential recordings using an algorithm described by Seamari and colleagues (Seamari et al., 2007). Sensory responses were classified according to those occurring during “Up” or “Down” states, including cases in which sensory stimulation triggered state transitions (Reig and Sanchez-Vives, 2007). Stimuli were given at regular intervals (0.2 Hz) and therefore the probability that they occurred at different periods of the cycle reflected the time spent by the network in up and down states. The membrane potential distribution during spontaneous activity shows a clear bimodal distribution in all recorded neurons (Figure S4, S7). Input resistance was measured as the slope of a linear fit between injected depolarizing and hyperpolarizing current steps and membrane potential. It has been described that MSNs have a prominent inward membrane rectification at hyperpolarized membrane potentials (Mahon et al., 2004; Nisenbaum and Wilson, 1995). In order to better quantify and measure this rectification we constructed four independent linear functions in response to the negative and positive steps delivered at up or down states. Evoked responses were measured and compared for up and down states. The onset of the evoked sensory responses was calculated as the average time between the stimulus trigger and the onset of the evoked potential of at

least 40 stimuli presented at 0.2 Hz. We used the first and second time derivative of the membrane potential to determine the onset and peak of the sensory response. Response amplitude was defined as the voltage difference between the peak and onset potentials and slopes were obtained as *dv/dt* between the onset and peak time interval. Unless mentioned explicitly, all statistical tests performed were paired or independent student's t-test following the Shapiro-Wilk normality test for all compared data points. Error bars presented in the graphs represent the standard error of the mean (SEM).

Anatomy.

Anterograde tracing. Both sex adult mice were anesthetized with intraperitoneal injection of ketamine and methodomidine, and placed in the stereotaxic as described above. All injections were made with glass pipettes (borosilicate, OD = 1.5 mm, ID = 1.18 mm) with a tip diameter of 5-10 µm. A total of 150–250 nl of BDA 10% (10,000 MW lysine-fixable biotin dextran amine, Molecular Probes) was dissolved in 0.9% NaCl and fast green (to aid visualization of the injected tracer). Injections were performed in layer 5 of BF and V1 using air pressure pulses. A single injection was done for each cortical area and animal using the coordinates described above, as taken from Paxinos and Franklin (2001). Following injection, we sealed the skin with surgical veterinary glue (3M Vetbond Veterinary Tissue Adhesive 1469SB). The analgesic carprofen (Rimadyl; Pfizer) was administered subcutaneously at 5mg/kg, and mice were awakened with intraperitoneal injections of a mixture of atipamezole (Antisedan; Orion Pharma; 1 mg/kg) and naloxone (0.1 mg/kg) diluted in 0.9 % NaCl. Mice were then returned to the animal facilities in separate cages. After 3-6 days animals were transcardially perfused with a solution containing 4 % formalin and 14 % saturated picric acid dissolved in 0.1 M phosphate buffer (PB, pH 7.4). Brains were extracted and stored in this fixative solution for 24-48 hours. Before cutting, brains were transferred into PBS containing 12 % sucrose for 24 hours. Coronal slices (20 µm thick) of both hemispheres containing the entire striatum (from AP 1.7 mm to AP -2.3 mm, following Paxinos and Franklin (2001)) were obtained using a cryostat and collected on gelatin coated slides. Sections were incubated over night with Cy3-conjugated streptavidin (Jackson ImmunoResearch Laboratories) and NeuroTrace 500/525 Green Fluorescent Nissl Stain (Invitrogen) diluted (1:1000) in 1 % BSA, 0.3 % Triton-X 100 in 0.1 M PB. Finally the glass slides were covered with glycerol containing 2.5 % diazabicyclo 2.2.2 octane (Sigma).

Morphological staining. At the end of each experiment the mouse was perfused and the brain was placed in fixative solution for 1-2 hours (same procedures and solution described above). After that, the brain was placed in a 0.01 M PBS and at the day before cutting it was maintained in PBS with 12%

sucrose. 10-12 µm thick coronal slices were obtained from the recorded hemisphere. Sections mounted on gelatin-coated slides were incubated overnight with Cy2-conjugated streptavidin (Jackson ImmunoResearch Laboratories) diluted (1:500) in 1 % BSA, 0.3 % Triton-X 100 in 0.1 M PB. In between all experimental procedures, slices were washed with 0.01 M PBS. We used fluorescent microscopy to find stained neurons. The shortest recording duration for a stained neuron was 24 minutes and the average was 55.44 ± 17.87 minutes (n = 45). Neurons were then reconstructed using a confocal microscope (Zeiss LSM 510 Meta).

Immunohistochemistry. Reconstructed striatal neurons were inmunolabeled for the detection of D_1 dopamine receptors, where we found MSNs that clearly expressed D_1 or not (D_1 n = 15; putative D_2 n = 13). Primary and secondary antibodies were diluted in 1 % BSA, 0.3 % Triton-X 100 in 0.01 M PBS. Sections were incubated between 48-60 hr at 4 °C with primary antibody diluted in 1:500 (D_1): Rat anti-D_1 dopamine receptor (Sigma-Aldrich). This antibody is selective for the 97 amino acid C-terminal fragment of human D_1. Sections were then incubated again for 60 min at room temperature with Cy3-conjugated affiniPure donkey anti-rat IgG (H+L) diluted 1:500 (Jackson Inmuno Research Laboratories). Finally, slides were mounted in glycerol containing an anti-fading agent. The slides were washed in 0.01 PBS at least 3 times for 15 min periods between each procedure step. We used fluorescent and confocal microscopy to recognize the MSN receptor expression (D_1). In order to visualize the results we used pseudo-color to represent the neurobiotin in red and the D_1 receptor expression in green. In order to control for the efficacy of the D_1receptor expression described above we stained slices from D2 EGFP mice, showing that somata of D2 expressing neurons were not stained by the antibody (Figure S5).

Image analysis. Photomicrographs of results were taken with Zeiss Axiocamp (Carl Zeiss AB, Stockholm, Sweden) or an Olympus BX51 (Olympus Sverige AB, Stockhom, Sweden) digital camera. Illustrations were prepared in Adobe Photoshop and Illustrator and images were only adjusted for brightness and contrast. Confocal Z-stacks of the slices were obtained using a Zeiss Laser scanning and mounted using ImageJ (Wayne Rasband, National Institutes of Health, USA).

References for Supplemental Information

Gong, S., Zheng, C., Doughty, M.L., Losos, K., Didkovsky, N., Schambra, U.B., Nowak, N.J., Joyner, A., Leblanc, G., Hatten, M.E.*, et al.* (2003). A gene expression atlas of the central nervous system based on bacterial artificial chromosomes. Nature *425*, 917-925.

Holtmaat, A., Bonhoeffer, T., Chow, D.K., Chuckowree, J., De Paola, V., Hofer, S.B., Hubener, M., Keck, T., Knott, G., Lee, W.C.*, et al.* (2009). Long-term, high-resolution imaging in the mouse neocortex through a chronic cranial window. Nature protocols *4*, 1128-1144.

Mahon, S., Deniau, J.M., and Charpier, S. (2004). Corticostriatal plasticity: life after the depression. Trends in neurosciences *27*, 460-467.
Nisenbaum, E.S., and Wilson, C.J. (1995). Potassium currents responsible for inward and outward rectification in rat neostriatal spiny projection neurons. The Journal of neuroscience : the official journal of the Society for Neuroscience *15*, 4449-4463.
Paxinos, G., and Franklin, K. (2001). The Mouse Brain in Stereotaxic Coordinates, 2nd edn (San-Diego, California: Academic Press).
Reig, R., and Sanchez-Vives, M.V. (2007). Synaptic transmission and plasticity in an active cortical network. PloS one *2*, e670.
Seamari, Y., Narvaez, J.A., Vico, F.J., Lobo, D., and Sanchez-Vives, M.V. (2007). Robust off- and online separation of intracellularly recorded up and down cortical states. PloS one *2*, e888.